Preprint

Ice-confined construction of a large basaltic volcano –Austurfjöll massif, Askja, Iceland

Graettinger, A.H [1]; McGarvie, D. W. [2]Skilling, I.P. [3]; Höskuldsson, A.H. [4], Strand, K. [5]

1University of Missouri Kansas City
2Lancaster University
3University of South Wales
4Haskoli Islands
5Thule Institute

Key words: Askja; glaciovolcanism; ice-confined; tindar; pillow lava; last glacial maximum

Corresponding author: Alison Graettinger graettingera@umkc.edu

Abstract

Austurfjöll is the largest basaltic glaciovolcanic massif at Askja volcano (Central Iceland), and through detailed studies of its volcanological and geochemical characteristics, we provide a detailed account of the sequence and structure of the ice-confined construction of a large Icelandic basaltic volcano. In particular, Austurfjöll represents a geometry of vents, and resulting glaciovolcanic morphology, not previously documented in ice-confined basaltic volcanoes. Austurfjöll was constructed during two major phases of basaltic volcanism; via seven eruptive episodes through disperse fissure-dominated eruptions. The earliest episode involved a rare and poorly-exposed example of subaerial activity, and this was succeeded by six episodes involving the eruption of ice-confined pillow lavas and numerous overlapping fissure eruptions of phreatomagmatic tephra. Evidence of local subaerial lavas and tephras indicates the local growth of eruptive centers above englacial lake levels, and subsequent flooding, but no prolonged subaerial activity. Localized ice-contact facies, paleowater levels and diamictons indicate the position and thickness of the ice was variable during the construction of Austurfjöll, and eruptive activity likely occurred in multiple and variable level melt-water lakes during the last glacial period. Lithofacies evidence including gradational transitions from effusive to explosive deposits, superposition of fragmental facies above coherent facies, and drainage channels suggest that changes in eruptive style were driven largely by external factors such as drainage and the increasing elevation of the massif. This study emphasizes the unique character of Austurfjöll, being composed of large pillow lava sheets, numerous (>40) overlapping glaciovolcanic tindars and only localized emergent deposits, as a product of its prolonged ice-confined eruptive history, contrasts with previous descriptions of tuyas and tindars.

Introduction

Iceland exists at the intersection of the Mid-Atlantic Ridge and the Iceland Hot Spot with volcanic activity producing monogenetic volcanic constructs and long-lived central volcanoes with associated fissure swarms (Einarsson 2008). Central volcanoes are large volume polygenetic volcanoes constructed by repeated eruptions in a localized area and frequently are characterized by bimodal volcanism (e.g. Eyjafjallajökull, Loughlin 2002; Katla, Lacasse et al. 2007; Krafla, Jonasson 1994). Askja is located in central Iceland and provides an opportunity to investigate the repeated interaction of basaltic eruptions at a central volcano with a thick ice sheet. Past work on basaltic glaciovolcanism in Iceland has concentrated on the products eruptions with focused vents that have produced tuyas, tindars, or conical subglacial mounds. Tuyas have distinctive flat topped and steep sided morphologies (Werner et al. 1996) and

tindars are linear ridges with slopes that dip away from the spine of the ridge (Schopka et al. 2006). These geometries dominate reviews of glaciovolcanic edifices (Hickson 2000; Komatsu et al. 2007; Russell et al. 2014; Edwards et al. 2015). Only a few studies have investigated polygenetic basaltic volcanoes that interacted with thick ice (Werner et al. 1996; Edwards et al. 2002; Smellie et al. 2008), which consequently limits our understanding of the life span, frequency of eruption, and eruption styles that occur at long-lived centers under ice. Askja, in central Iceland, contains multiple exposures of the internal stratigraphy of a polygenetic basaltic center that interacted with thick glacial ice (Sigvaldason 1968). Askja does not have a typical tuya or tindar morphology like previously described central volcanoes (Herðubreið; Werner et al. 1996). Askja comprises four glaciovolcanic massifs, at least three calderas, ample Holocene basaltic lavas, and lesser volumes of silicic volcanic including the 1875 plinian eruption deposit (Sigvaldason 1968; Carey et al. 2009; Hartley et al. 2016). This paper describes the deposits and geomorphology of the Austurfjöll massif (Figure 1) that makes up the eastern wall of the 1875 caldera. Austurfjöll is the largest glaciovolcanic massif at Askja reaching 750 m above the surrounding landscape, has an area of 48 km^2, and is constructed largely of pillow lava sheets, pillow mounds, and overlapping fissure ridges (or tindars), that are dominantly composed dominantly of glassy phreatomagmatic tephra. While these facies are typical of basaltic eruptions into ice-confined lakes, the topography of the massif steps down in a series of ridges and valleys towards the east, away from the caldera rim, representing repeated basaltic eruptions in multiple and variable volume ice-confined lakes.

Austurfjöll was investigated using a combination of field-based lithofacies descriptions, geomorphology, and geochemical data. The degree of preservation, a lack of major erosional surfaces, and an absence of extensive glacial diamictite deposits suggests that Austurfjöll was produced during the last (Weichselian) glacial period. Detailed lithofacies analysis shows the dominance of ice-confined fissure eruptions of phreatomagmatic tephra over extensive pillow lava sheets, the collapse of unstable edifices, and subsequent transport and deposition of material in water. Local deposits of subaerially emplaced pyroclastic deposits and lava flows reveal the variable nature of the water level within ice-confined lakes. Intrusions are a common feature in coherent and fragmental lithofacies and provide additional evidence about the emplacement environment. The recognition of seven eruptive units, through stratigraphic relationships including two diamictite units supported by geochemical trends, indicates that the construction of Austurfjöll involved multiple ice-confined eruptions and vents in multiple lakes. This growth model introduces a new level of complexity to the way that large long-lived basaltic volcanoes grow in the presence of thick ice sheets. This model has implications for the stability

of an ice sheet over a productive volcanic edifice without a centralized vent, such as the presence of multiple meltwater lakes that can vary in size and distribution through time and erosive drainage events (Smellie 2006). Furthermore, this newly described morphology is relevant for studies of glaciovolcanic constructs on Mars that are dependent on terrestrial analogs and topographic data (Ghatan and Head 2002; Houvis et al. 2008; Martinez-Alonso et al. 2011).

Methods

Field work focused on lithofacies descriptions, structural measurements, and sample collection, and was supplemented by ground and aerial-based photographic documentation. Lithofacies descriptions include bed thickness, sedimentary structures and contacts, clast type, clast shape and clast size as documented in the field and supplemented by observation of samples. The partially lithified nature of the deposits throughout the massif precluded the use of traditional granulometric analyses. Consequently, maximum and median clast sizes were manually measured in the field and corroborated with photographs. Vesicularity was visually estimated in the field and from thin sections using ImageJ.

The distribution of lithofacies was mapped using available exposures and stratigraphic logs, and then extrapolated to areas of poor/zero exposure and where access was difficult (e.g. along the actively collapsing caldera wall) (Graettinger et al. 2013a). Twenty-three stratigraphic logs were drafted and these were used to reconstruct the relationships between lithofacies and to document stratigraphic and erosional boundaries within Austurfjöll (Figure 1). Most logs were collected in steep-sided gullies. An additional 19 logs collected by Strand and Höskuldsson in 1980 for NORVOLK (Strand 1987) around the caldera rim were used to supplement the new logs.

Bulk rock geochemical analyses of 57 rock samples were conducted using X-Ray Fluorescence spectroscopy (XRF) at McGill University (Montreal, Canada) and Washington State University GeoAnalytical Lab (Pullman, USA). Samples analyzed were from coherent facies including pillowed and non-pillowed lavas, intrusions, and lava clasts within fragmental units within recognized stratigraphic units as part of a complete facies characterization (Cas and Wright 1987). Samples with visible alteration or zeolites were avoided. Repeat analyses of samples from a single stratigraphic unit were used to establish the variability of unit chemistry. Once established, the geochemical signatures were used to aid stratigraphic correlation of eruptive products that were not laterally continuous and map these units across the massif.

Lithofacies

Glaciovolcanic lithofacies were divided into ash tuff, lapilli tuff, breccia, and lavas. Subdivisions of these lithofacies were based on componentry and sorting. Macro-phenocrysts of plagioclase are common in some deposits and are noted as a characteristic trait for identification in the field (an x is added to the lithofacies code), but as porphyritic units do not otherwise vary from similar lithofacies lacking crystals they are not discussed separately (Table 1).

Lavas

Coherent lithofacies (lavas) are divided into pillowed and non-pillowed groups, and interpreted to be subaqueous or subaerial based on internal and surface textures. Pillowed lavas are far more common than non-pillowed lavas, and were subdivided into two facies based on the size and regularity of the stacking of pillow lava tubes. Regular pillows (Pl1) range in size from 10-50 cm in cross-sectional diameter with elliptical shapes. The similarity in pillow diameters results in organized stacking of pillow tubes. Irregular pillow lavas (Pl2) range in size from 5-200 cm in cross-sectional diameter, which produces irregular stacking of pillow shapes interspersed with local zones of columnar or entablature jointing between pillow tubes. Vertical pillows and mega-pillows (≥200 cm in cross-section) are observed locally in irregular pillow lavas.

Non-pillowed lavas occur in small outcrops with extents no greater than a few tens of meters and they are assigned to two groups: vesicular entablature-jointed lavas (L1) and dense reddened lavas with locally scoured scoriaceous tops (L2). L1 lavas can transition laterally into Pl1 pillowed lavas. Some L1 lavas exhibit radial fractures that extend through the flow. L2 lavas have a distinct red coloration and locally present scoriaceous tops and/or surface scours. In thin section, the L2 lavas have an abundance of oxide microlites absent in all other facies.

Interpretation

The bulk of lavas observed at Austurfjöll (Pl1, Pl2 and L1) have characteristics typical of subaqueous lavas such as pillow morphologies, entablature fracturing, and/or thick chill rinds (Dimroth et al. 1978; Gregg and Fink 1995; Smellie and Hole 1997; Kennish and Lutz 1998; Goto and McPhie 2004; Tucker and Scott 2009). Pillow lavas (Pl1 and Pl2) represent a low effusion rate whereas sheet lavas (L1) represent higher effusion rates (Gregg and Fink 1995; Parfitt et al. 2002; Gregg and Smith 2003). There is no correlation between phenocryst abundance and lithofacies assignment (Pl1, Pl2), and field estimates of vesicularity varies

between 30-70% for both facies. Both pillow facies occur at multiple locations around the massif, at variable distances to candidate vents, and can be traced laterally for tens of meters, suggesting this difference is not simply controlled by distance from a vent. Rather, we suggest, the changes in pillow lava morphology at Austurfjöll are dependent on the lava-supply rate, and not variations in viscosity due to cooling (Walker 1992). As such, the irregularity of Pl2 lavas are interpreted to represent an end-member of pillow style effusion, where a minor increase in eruption rate results in the development of textures transitional to lobate flows, such as larger lobes, and presence of entablature jointing. L2 non-pillowed lavas are interpreted to be subaerial in origin, showing significant evidence of interaction with oxygen (oxide microlites and red color). Where present, the local scoriaceous top implies that the flows had a'a structures and were likely eroded by glacial activity that removed the top and produced observed scours.

Breccias and diamictites

Breccias and diamictites are common at Austurfjöll and are differentiated by clast type and shape as well as sorting. This lithofacies include pillow and fluidal bomb breccias (B1), angular block breccias (B2), red lava fragment-bearing breccias (B3), and glacial clast-bearing diamictites (Dia1 and Dia2). Deposit color is influenced by the abundance and degree of palagonitization of ash-sized matrix material.

Breccias

Pillow and fluidal bomb bearing breccias (B1) are typically clast-supported with clasts 7-70 cm in diameter, and contain recognizable pillow forms, pillow fragments, and/or fluidal bombs (Figure 2a). Some clasts have distinctive glassy rims 2-10 mm thick. There is no regular structure to these deposits, and they can transition laterally and vertically into pillow lavas (Pl1 and Pl2). The matrix is dominated by lapilli-sized angular vitric particles with local concentrations of coarse ash. Vesicularity of the lapilli (from visual estimates) is variable, but is typically between 10-30% in hand samples and thin sections. Pillow breccias (B1) are often cut by dikes of various morphologies.

Angular block-bearing breccias (B2) are clast- to variably matrix-supported (Figure 2b). These breccias display zones of clast concentrations, but not bedding. Clast size and matrix variation in angular breccias are similar to B1 breccias, but the clast shapes are notably angular. Red lava fragment breccias (B3) occur typically in thin (<1 m) lenses between lapilli tuffs and subaerial lavas along the caldera rim. B3 breccias contain distinctive clasts of dense red-hued lava (L2) and red scoria. Other clasts in B3 breccias include microcrystalline lava, porphyritic

lava, and lithified ash tuff. B3 breccias are clast- or matrix-supported. The breccia matrix consists of coarse ash and lapilli, with a wide range of vesicularities and particle shapes.

Interpretation

Breccias are a common feature in glaciovolcanic settings and are produced in a variety of eruptive and post-eruptive conditions. There are many mechanisms for producing clast-supported breccias, including: collapse, flow-generated breccias, explosion, and disruption by intrusions (peperite formation or destabilization; Carlisle 1963; Dimroth et al. 1978; Loughlin 2002; Sansone and Smith 2006; Vezzoli et al. 2008; Edwards et al. 2009; Skilling 2009; Tucker and Scott 2009; Mercurio 2011; Kralj 2012; Watton et al. 2013). The nature of the clasts in conjunction with field relationships helps differentiate between breccias formed by either explosive, intrusive, or gravity-driven processes. Breccias at Austurfjöll (B1, B2, and B3) show similar textural characteristics in terms of clast-support, clast size range, and deposit thickness, but each facies has distinct clast types. B1 breccias contain unequivocal clasts of intact and fractured pillows and in some cases fluidal bombs, and therefore contain primary or only slightly reworked eruptive products. They are interpreted to be the result of explosive processes near or through pillowed lavas, and/or the collapse of pillowed lava flow margins. In contrast, B2 and B3 are associated with angular blocks that may be of ballistic, but more commonly, gravitational origin. Blocks in B3 are interpreted as fragments of broken subaerial lava (L2), with oxidation staining and occasional scoriaceous textures. B1 and B2 breccias are associated with pillowed and non-pillowed lavas at a range of elevations. B3 breccias occur predominantly at higher elevations along the caldera rim and outward directed dips indicate that the breccias likely have a source somewhere in what is now the caldera.

Diamictites

Two diamictite lithofacies occur at Austurfjöll. Rounded cobble diamictite (Dia1) is moderately lithified and contains diverse clast lithologies that are well-rounded with scoured and polished surfaces. The clasts are supported by a grey-brown fine ash matrix, distinct from breccia matrix in both color and dominance of sand and silt sized material (Figure 2c). The deposit is poorly-sorted and is massive in structure. Outsized clasts and matrix components both include low to highly vesicular clasts of lava with variable crystal populations. Clasts of palagonitized tuff are rare, and where present are pebble-sized or smaller. Deposits of Dia1 are typically on the order of one meter thick, and do not occur in beds or have consistent contacts.

This lithofacies is not laterally continuous beyond a few meters, locally mantles vertical exposures, and is disrupted by pillowed intrusions.

Matrix-supported pebble diamictite (Dia2) has centimeter-scale bedding and contains subrounded to rounded clasts supported in a grey-brown fine ash matrix (Figure 2d). Clasts are typically small cobble to pebble-sized and may display glacial polish or striations. Outsized clasts are diverse, but dominant clast types include dense and vesicular lava. The diamictite is typically on the order 50 cm or less in thickness, and has a sub-horizontal upper surface that may extend several hundred meters along the southeastern margin of Austurfjöll. The Dia2 lithofacies overlies lavas exhibiting glacial scour.

Interpretation

Dia1 is a massive deposit that contains clasts with distinctive glacial signatures, such as surface scours. The concentration of glacially altered clasts, sorting, and massive nature indicates that the deposit is either glacial in origin or reworked from a glacial deposit. Descriptions of glacial deposits at glaciovolcanic centers are limited (Bergh and Sigvaldason 1991; Loughlin 2002; Bennett et al. 2006; Smellie 2008; Carrivick et al. 2009) partly because the lithologies available for incorporation into diamicts are so similar in Iceland. The lack of lateral continuity of the deposits described at Austurfjöll suggests that these deposits are not regional-scale glacial till deposits, but either localized lodgment tills, moraine deposits, or related to subglacial fluvial transport. The extent of these deposits is difficult to constrain due to incision of younger gullies. Some of the Dia1 deposits are also disrupted by intrusions and/or loading from overburden. Intrusions with convolute morphologies into Dia1 indicate volcanic activity resumed, or was active, when deposits were unconsolidated. Intrusions and stratigraphic relationships suggest Dia1 deposits were emplaced before and between the first two pillow lava eruptive units at Austurfjöll. The more continuous distribution, finer grain size and bedding of Dia2 suggest that they are localized glacial outwash deposits, where the glacially deposited material was fluvially remobilized by meltwater at the base or front of the glacier. The narrow distribution of diamictite deposits between subaqueous eruptive deposits, suggests that the diamictites do not represent a prolonged hiatus in eruptive activity.

Lapilli and Ash tuff

The most voluminous lithofacies at Austurfjöll are the ash and lapilli tuffs, making up almost 50% of the total massif volume. These are distinguished from each other by clast morphology and componentry. Deposit color is influenced by the abundance and degree of

palagonitization of ash-sized material. Angular vitric lapilli tuff (Lt1) is massive and can display variable amounts of matrix palagonitization. Occasional fluidal bombs reach up to 50 cm in diameter (Figure 3a). The deposit is poorly sorted and lapilli-supported, with occasional fine ash matrix, and can display a weak upward fining. These deposits are described and interpreted in detail in Graettinger et al. (2013b). Subrounded lapilli tuff (Lt2) contains distinctive subrounded blocks in a lapilli-dominated matrix. Lapilli are 1-6 cm in diameter. Blocks are sub-angular to rounded and up to 30 cm in diameter. Typical blocks include vesicular to non-vesicular rounded lava that can occur in concentration zones of, but with no regular bedding. The facies is otherwise poorly sorted (Figure 3b). Red scoria lapilli tuff (Lt3) contains subrounded lapilli with distinctive clasts including red scoria and armored lapilli (Figure 3c). The deposit is clast- or matrix-supported with outsized clasts of bombs/bomb fragments. Lt3 is the only lapilli facies to contain rare bomb sags. Heterolithic lapilli tuff (Lt4) facies contains little to no fresh glass in a highly heterolithic subrounded to rounded lapilli-dominated tuff. Clast composition includes dense and vesicular lavas, red scoria, and consolidated blocks of ash tuff. The deposit is supported by a coarse ash matrix. Blocks are up to 20 cm in diameter (Figure 3d).

Massive coarse ash tuff (At1) is composed of predominantly coarse ash and forms beds that are frequently thick (>5-50 m), displaying occasional blocks of lava fragments. Thin localized zones of weakly bedded material are uncommon (Figure 4a). Bedded to laminated ash tuff (At2) contains coarse ash, fine ash, and occasional very fine ash beds that are well-sorted. Laminations occur on the scale of <2 cm within beds having a maximum thickness of 2 m. Occasional millimeter- to centimeter-thick very fine ash layers occur (Figure 4b). Alternating bedded ash tuff (At3) consists of well-sorted coarse ash beds of 5-50 cm thick, that are inter-bedded with fine ash beds of 3-15 cm thick. Weak centimeter-scale sedimentary structures such as cross-bedding, ripple marks, and normal grading also occur. Overall At3 deposit thickness can vary from a few centimeters to >15 m thick (Figure 4).

Highly deformed domains, or packets, of vitric ash to lapilli tuff (At4) are a common feature in the field area. These domains occur at all elevations, and overlap all other lithologies. At4 deposits comprise domains of coarse ash-dominated, bedded sediment that display both meter-scale folding and centimeter-scale convolutions (Figure 5). These deformed sediment domains display preserved internal bedding, lamination, and sedimentary structures (including scours, cross-bedding, and ripples), but the packets of sediment in most cases display a steeply dipping orientation and are folded at high angles (tilted bedding is as high as 85^0). Individual beds are centimeters thick (5-10 cm average), with varying clast sizes from fine ash, to coarse ash, and lapilli up to 4 cm. Clasts vary from subrounded to rounded lapilli, to <10 cm diameter

angular blocks of dense to vesicular lava. Packets of At4 range from 20-200 cm thick. Contacts with surrounding beds are typically very sharp, but transitional boundaries with undeformed beds of At2 and At3 are observed.

Interpretation

The Austurfjöll ash and lapilli tuff deposits are dominated by Lt2 and At1 facies. These two lithofacies are dominated by subrounded to subangular, poor to moderately sorted particles that may be weakly bedded or massive. The rounding of clasts and, more importantly, the development of local sedimentary structures is indicative of transport in water following eruption. Bedding, cross-stratification, ripple marks, and loading structures are most common in the ash-dominated facies. Lapilli tuffs with poor sorting and lack of sedimentary structures represent rapid deposition of large volumes of highly-concentrated material (Maicher et al. 2000). The occurrence of increased bedding and traction current structures in more distal ash tuff deposits (At2) is consistent with sediment gravity flows described from subaqueous eruptive centers (White 2000). Subaqueous density current deposits dominate the deposits of other glaciovolcanic and submarine volcanic centers (Maicher et al. 2000; White 2000; Schopka et al. 2006) and are considered the likely mechanism of emplacement for these facies. Thick (20 m) and massive deposits such as At1 may represent deposits that were rapidly emplaced without significant remobilization. However, palagonitization, a common process in vitric basaltic deposits, can mask evidence of bedding or other fine structures - particularly in ash-dominated deposits (Stroncik and Schmincke 2002). This is observed in partially palagonitized ash-dominated deposits at Austurfjöll. The Lt1 facies is the only example of primary subaqueous fall out, or direct settling of pyroclastic material from an explosion of coarse material, identified at Austurfjöll. These deposits are distinguished by a high degree of angularity of all grain sizes, preserved fragile glassy particles, a gradational upward fining, and fluidal bombs (Graettinger et al. 2013b).

The steep slopes of unconsolidated deposits that comprise glaciovolcanic piles are conducive to collapse, and can produce deposits with similar characteristics to eruption-fed density currents (Sansone and Smith 2006). The regular bedding and frequent presence of sedimentary structures such as ripples and loading structures within At2 and At3 are indicative of either low energy density currents (distal flows of eruption-fed currents) or the gravitational remobilization of previous deposits. Distinguishing between these deposits depends on slope and stratigraphic relationships. Measured slopes of At2 and At3 deposits are typically between 10^0 and 25^0. Deposits at steeper angles (ca. 20^0) likely indicate distal deposits of eruption-fed

density currents that were not remobilized. At2 deposits on shallower slopes most commonly occur in large packets up to 40 m thick and fill large (100 m wide) channel forms, suggesting a remobilized history. This indicates that there was significant remobilization of deposits at Austurfjöll.

Lt3 and Lt4 facies contain more diverse components than Lt1-2 and At1-3, and have a limited distribution along the margin of the caldera at high elevations (Figure 1) with dips that radiate away from the caldera rim. These facies sometimes contain subaerially-derived clasts such as red scoria and blocks of subaerial lava. Lt3 contains armored lapilli, which likely formed above the water level, and could be emplaced subaerially or in calm and shallow subaqueous environments (McPhie et al. 1993; White 1996). Additional support for a shallow water interpretation occurs in rare bomb sags in this lithofacies. The Lt3 facies is, therefore, interpreted as an indicator of shallow or subaerially-emplaced emergent deposits. Lt4 contains a combination of subaerially- and subaqueously-derived clasts, suggesting the remobilization of subaerial deposits in an erosive traction current or through collapse to incorporate both clast types. The dominance of these facies along the caldera rim suggests a lake level near this elevation. Further evidence of such a lake level has been lost to the caldera subsidence event that removed the westernmost sector of the Austurfjöll glaciovolcanic massif.

Deformed domains of At4 occur at multiple elevations on all other lithofacies at Austurfjöll. The fairly fine (centimeter-scale) bedding of the domains, including ripples and channel forms, indicate that they are likely the result of small subaqueous gravity flows. The modern steep angles and deformation of these deposits suggests partial collapse of the underlying deposits, or slumping at the margin of pillow lava flows or sediment piles. The preservation of both sharp contacts and local transitions into undisturbed beds supports a collapse origin for the deformation. The commonality of these features only further underline the instability of growing piles of volcanic deposits within ice-confined lakes.

Intrusions

Intrusions are common in glaciovolcanic complexes, and Austurfjöll is no exception. Basaltic dikes intrude both pillowed and fragmental host materials. Dike morphologies vary from narrow tabular dikes of 50 cm in diameter to complicated pillowed dikes and coherent margined volcaniclastic dikes (CMVD) 1 to 3 m in diameter (Graettinger et al. 2012). Intrusions were frequently found at the center of linear tindar ridges composed of fragmental material with peperite or sharp contacts with the host material.

Interpretation

The pillowed, convolute, and tabular intrusions observed at Austurfjöll are similar to those described in other glaciovolcanic centers (Edwards et al. 2009; Skilling 2009). The dike morphologies provide important information about the environments at the time of their emplacement (Schopka et al. 2006; Edwards et al. 2009; Stevenson et al. 2009). Tabular dikes are typical of basaltic volcanic centers where magma interacts with competent rock and lithified deposits (Baer 1995; Rivalta and Dahm 2006). These dikes can serve as feeders for eruptions, or they may be arrested on the way to the surface. Pillowed dikes and peperitic margins are indicative of intrusion into unconsolidated, and typically wet, sediments (Walker 1992; Doyle 2000; White et al. 2000; Skilling et al. 2002; Mercurio 2011). CMVDs are interpreted as the result of magma interacting with ice-cemented sediments (Graettinger et al. 2012), and although they have not yet been described at other tuyas or tindars, they are expected to be common in ice-confined volcanic centers.

Lithofacies associations

The bulk of Austurfjöll is composed of coherent and fragmental deposits erupted in contact with water and ice. The rarity of subaerial deposits indicates that abundant water was present in ice-confined lakes during the construction of Austurfjöll. The facies associations can be grouped into three major constructs: tindars, thick pillowed lava flow sheets, and pillow mounds. Depositional centers of reworked material occur between these constructional features. The constructive lithofacies are typically ordered into localized sequences of pillow lava and pillow breccia (Pl1, Pl2, B1) or subaqueous lavas and related breccias (L1, B2), overlain by fragmental deposits of ash and lapilli tuffs (Lt1, Lt2, At1) (Figure 6). Roughly, Austurfjöll is composed of large pillow lava sheets overlain by stacked and overlapping tindars, with local pillow mounds. Deposits of remobilized fragmental material accumulate in topographic lows and as channel fills between eruptive vents (At2, At3, At4). Many of the depo-centers are cross-cut by dikes, indicating that intrusion, primary and reworked deposition were all broadly contemporaneous.

Tindars

The most common eruptive construct exposed on Austurfjöll are glaciovolcanic fissure ridges, also known as tindars. Tindars are linear ridges composed of fragmental volcanic material with slopes that dip away from the spine of the ridge. These tindars are distinguished from tuff cones as they do not present quaquaversal (circular radially outward dipping)

structures and instead are linear features with beds dipping away from the ridge axis. The linear ridge of fragmental deposits with an intrusive core is typical of tindars described from numerous locations in Iceland and British Columbia (Werner and Schmincke 1999; Schopka et al. 2006; Edwards et al. 2009; Jakobsson and Gudmundsson 2008; Mercurio 2011; Pollock et al. 2014). Tindars have also been described composed predominantly of pillow lavas, but presenting a linear morphology (Werner and Schmincke 1999; Höskuldsson et al. 2006; Edwards et al. 2009; Pollock et al. 2014). Austurfjöll tindars are composed predominantly of ash and lapilli tuffs (Lt1, At1, Lt2, At2) and are, in most cases, cored with a feeder dike that may have a tabular and/or pillowed morphology (Figure 7a). In some tindars, basal pillow lavas and pillow breccias are partially exposed. Unlike the isolated tindars that occur in fissure swarms around Iceland, Austurfjöll tindars occur in close proximity and overlap each other. Tindars at Austurfjöll are typically 300 m in length and 50 m high relative to surrounding terrain. Typical fissure swarm tindars have a length of twice the width of the ridge (Jakobsson and Gudmundsson 2008), and these same proportions apply to most Austurfjöll tindars. Additionally, the Austurfjöll tindars occur in large numbers and are constructed predominantly on top of previous eruptive constructs. This study has identified over 40 individual tindars currently exposed at Austurfjöll, with an unknown number of buried tindars (Figure 8). The presence of numerous closely spaced and locally overlapping tindars produces the prominent stepped appearance of Austurfjöll. This is augmented by the infill of topographic lows between ridges by primary and remobilized ash and lapilli tuffs. Some of the inter-tindar depo-centers contain large channel structures up to 100 m across, suggesting that the deposits were eroded rapidly during and/or soon after their formation (Figure 7b).

Pillow lava sheet

Pillow lava sheets form the base of Austurfjöll and are only exposed at low elevations, particularly along the southeastern sector (Figure 1). The sheets can extend up to 1 km in length with individual sheets up to 60 m thick and typically have distinctive sub-horizontal tops (Figure 7c). Exposed interiors of these sheets indicate they are composite and comprise multiple pillowed lava flows, with local marginal breccias (B2). Individual flows within a pillow lava sheet can be made up of Pl1 or Pl2 lavas and local lobate lava flows (L1). These three facies can show either gradual transitions or sharp contacts. Pillow lava sheets may be stacked, with pervasive sub-horizontal contacts typically associated with a change between Pl1 and Pl2 facies. A few examples of vertical pillows at the contact between individual flows suggest that the pillow lava sheets may have locally interacted with the confining ice, or a thin meltwater lens

between the flow front and the ice (Hungerford et al. 2014). Steep-sided gullies incised into the southeastern sector reveal that stacked pillow lava sheets are up to 100 m thick. The plateaus associated with the top of pillow lava sheets are buried by overlapping tindars and less common pillow mounds. No vents for the pillow lava sheets are exposed, but the dominance of fissure-controlled geometries at Austurfjöll (Figure 8) suggests that they may have also been fissure-fed.

Pillow mounds

Pillow mounds are less common but widespread, and are generally no more than a few tens of meters in size and 15-30 m thick. They occur stratigraphically above the major pillow lava sheets and form steep slopes between 40-50 degrees (Figure 7d). These mounds are constructed of Pl1 or Pl2 facies pillowed lava flows. The bases of the mounds are frequently buried by local detritus and/or pyroclastic deposits from the AD 1875 eruption. The pillow mounds typically occur on shallow slopes of ~10 degrees. Pillow mounds occur either as clusters, or as a single mound and display circular footprints. These constructs reflect entirely effusive subaqueous eruption histories, and are limited in size at Austurfjöll to a few tens of meters in diameter. These features contrast with conical features composed of predominantly pillows and interstitial breccias and tuff, referred to as subglacial mounds described up to 2 km in diameter in British Columbia, Canada (Hickson 2000). The size limitation at Askja may be related to the abundance of fissure-type vents, rather than a focused vent.

Subaerial deposits

The lowest stratigraphic deposits exposed at Austurfjöll are glacially scoured subaerial lavas. The lavas have limited exposures, but appear to be laterally extensive (~30 km^2). All other subaerial deposits occur only locally, most frequently as clastic deposits containing subaerial components (i.e. B3, Lt3, Lt4). Pyroclastic (Lt3) and effusive (L2) deposits occur around the caldera rim at elevations greater than 600 m above the local base level (1250-1450 m asl) representing the highest preserved modern elevations of Austurfjöll (Figure 1). These deposits are surrounded by subaerial clast-bearing breccias and tuffs (B3, Lt4) that suggest the primary subaerial deposits were emergent and partially remobilized down slope to be deposited in shallow water. The only examples of bomb sags at Austurfjöll occur in these remobilized deposits near the caldera rim. As these features occur in the absence of confining topography, they likely represent a maximum ice-confined water level during late stage construction of Austurfjöll.

462 Three other locations of subaerial deposits were found on Austurfjöll and are
463 interbedded with subaqueous deposits. These isolated subaerial lavas occur at lower elevations
464 and cover less than 1 km^2 each. These lavas occur at roughly 560-600 m above the local base
465 (1160-1200 m asl) and occur in the NW, NE and SE sectors of Austurfjöll (Figure 6). These
466 lavas probably indicate fluctuations in the levels of ice-confined lakes during the construction of
467 Austurfjöll. These fluctuations may be associated with temporary drainage, or emergence of
468 eruptive vents. Both scenarios require a subsequent increase in lake level to produce
469 subaqueous lavas on top of the subaerial lavas and serve to illustrate the typically dynamic
470 nature of water levels during construction of glaciovolcanic edifices (Skilling, 2009).
471
472 *Glacial and fluvial deposits*
473 Local matrix-supported diamictites containing glacially polished clasts are interpreted as
474 either local glacial tills or locally reworked till material. Local interaction with ice (till, vertical
475 pillows, radial cooling cracks on lavas, glacial scour and glacial erratics) indicates that the ice
476 margin was at times close to, or covering some of the eruptive deposits. The glacial deposits,
477 however, do not form extensive horizons that would indicate a prolonged hiatus between
478 eruptive events, or major recursions of ice over the massif, suggesting that Austurfjöll was likely
479 constructed entirely during the last glacial period (Weichselian).
480 Fluvial deposits are located predominantly in depositional centers between tindar ridges
481 and pillow mounds. The At2 and At3 facies are interpreted as reworked material from
482 subaqueous eruptions because of their dominance of sedimentary structures and low angle
483 bedding. The eruption of fine-grained material onto steep slopes in a subaqueous environment
484 is conducive to remobilization. Rare examples of large drainage channels suggest that the
485 volume of water within the ice-confined environment may have changed rapidly and reworked
486 large volumes of sediment quickly (Figure 7b). The occurrence of localized subaerial deposits at
487 lower elevations in the massif that transition laterally into subaqueous deposits support falling
488 lake levels (Smellie 2006; Russell et al. 2013)
489
490 **Geochemical Data**
491 Whole rock geochemistry of 54 volcanic rocks from Austurfjöll lavas, dikes, and blocks
492 from fragmental deposits (Pl, L, B, Dia, and Lt) was undertaken. The purpose was to determine
493 the compositions of erupted melts produced during the construction of Austurfjöll to provide
494 insight into the range of compositions produced during pre-Holocene period. The geochemistry

was also leveraged to support stratigraphic relationships where physical connections between eruptive units was either lacking or obscured, a common issue in glaciovolcanism.

All 54 volcanic rocks analyzed are basalts on the basis of SiO_2 contents (i.e. 48-52%; Figure 9), and normative mineralogy indicates that these basalts are tholeiites, with 21 being quartz tholeiites and 33 being olivine tholeiites. Similar basalt compositions have been reported for Holocene basalts at Askja (Macdonald et al., 1987; Kuritani et al., 2011). The common occurrence of quartz tholeiites at Icelandic central volcanoes located in the active rift zones has long been recognized (Wood, 1976, 1978), where slightly more evolved melts are generated in comparison to the offshore spreading segments of the Mid-Atlantic Ridge.

The geochemical characteristic of the erupted basalt was also used as means of corroborating the primary stratigraphy of Austurfjöll based on field mapping. The geochemical character of eruptive units was established by first grouping stratigraphically known samples, and then evaluating the variability within each unit. This ensured that the primary stratigraphy, established by field mapping, took precedence. Once established, the geochemical signatures were then used to correlate eruptive products that are not laterally continuous (Figure 9) and map these eruptive units across the massif (Figure 10).

To test this, 23 samples from a single and extensive pillow lava sheet (Unit 2) were analyzed, and the results are shown in Table 2, where the variability of Nb (17-20 ppm) and Y (34-42 ppm) are small, whereas the ranges for Rb (2-14 ppm), Zr (150-172 ppm) and Ce (31-57 ppm) are greater. Note also that the ratios of incompatible trace elements show similarly low variability, with Y/Nb, for example, varying from 1.8 to 2.5, with 21 of the 23 samples lying in the range 1.9-2.2. Similar relationships are seen in Rb/Nb and Zr/Nb ratios, with the bulk of analyses lying within a restricted range (Table 2). This process established that 23 samples from one well-defined eruptive unit possess a suitably narrow range of compositions to enable the correlation of stratigraphic units when physical connections were missing or obscured. Samples whose stratigraphic relationships were uncertain were then assigned to one of the Units by matching their trace element characteristics to a specific Unit. This proved to be relatively straightforward to do, as each Unit was observed to have its own subtle but distinctive geochemical characteristics, most clearly expressed in the relative concentrations of the trace elements Nb, Rb, Y, Zr, and Ce (Table 3). The relative enrichment of these six incompatible elements shows the distinctive signature of the units (Unit 6<Unit5<Unit4<Unit1<Unit2 <Unit3<Unit7). The complete dataset is available as Online Resource 1.

This supplementary geochemical corroboration enabled a refined eruptive history of Austurfjöll that reinforced field observations including the large extent of pillow lava sheets (Unit

2) and the limited extent of some eruptive units (Unit 4 and 7). Additionally, this process revealed the presence of Unit 2 clasts within diamict (Dm2) enhancing the rich stratigraphic story preserved at Austurfjöll.

Eruptive history of Austurfjöll

The stratigraphically lowest unit of Austurfjöll occurs at an elevation of 600 m asl and comprises glacially scoured subaerial a'a lavas (Unit 1). There is a locally exposed erosional boundary between the Unit 1 subaerial lavas and the overlying glacial diamictite (Dm 1), which is overlain by the first pillow lavas (Unit 2). Basaltic activity occurred while the glacial deposits were still unconsolidated as there are complex intrusions and peperites cross-cutting the diamictites. The earliest glaciovolcanic activity at Austurfjöll involved the formation of Unit 2, which is a ca 10 km^2 and 1 km^3 pillow lava sheet covered by tindars and remobilized tuff. The fragmental deposits were emplaced on top of the pillow lava sheet above 700 m asl. Locally this unit was erupted into subaerial conditions (Figure 6), but subaqueous deposits immediately above and laterally transitional to these exposures suggest that these deposits do not represent a permanent or long-standing lake level. Unit 2 lavas also experienced local post-emplacement interaction with ice as evidenced by the presence of vertical pillows along flow margins recording the retreat of a confining ice wall, as well as local scour and large isolated blocks of lava and tuff on topographic highs that are likely glacial erratics. Additionally, the presence of local diamictite (Dm 2) indicates that ice was present during and after the eruption. The diamictite contains clasts of Unit 2 lava which is evidence of a local advance of the ice mass leading to partial erosion of Unit 2.

After the emplacement of the diamictite, basaltic activity re-initiated with a more limited distribution of effusive pillow lava sheets (Unit 3). This was then followed by numerous explosive fissure eruptions producing a series of tindars, local subaqueous lava flows, and inter-ridge depositional centers (Units 3 and 4). This was followed by Unit 5, comprising the most voluminous episode of tindar formation. Near the caldera rim this unit contains heterolithic lapilli tuffs that include both subaerially and subaqueously erupted clasts (Figure 6). This was followed by the localized subaqueous eruption of Unit 6 porphyritic pillow mounds that drape over the northeastern corner of Austurfjöll from 1160 m asl to the base of the massif (600 m asl). This unit contains local examples of lava-ice interaction in the form of laterally confined radially fractured lava flows. The uppermost unit of Austurfjöll is Unit 7, which is composed entirely of localized subaerial lava breccias sits on the caldera rim.

562 The eruptive unit map (Figure 10) and constructional features of the massif can be used
563 to extrapolate potential cross-sections of the massif (see Online Resource 2). The
564 predominance of subaqueous textures preserved by these deposits indicates the presence of a
565 recurring ice-confined meltwater lake or lakes that were subject to drainage and refilling events
566 (Figure 11).
567 Based on observations at Austurfjöll it is likely that basaltic glaciovolcanic activity within
568 thick ice sheets (>700 m ice as constrained by the thickness of subaqueous deposits) initiated
569 with the formation of large pillow lava sheets with associated local breccias. This activity was
570 followed by the eruption of overlapping tindars as explosive activity increased as Austurfjöll built
571 up and confining pressures above newer vents were commensurately reduced. This phase
572 likely occurred in a large open ice-confined lake, if one was not already present (Figure 11).
573 The abundance of fissure-controlled geometries suggests that all eruptive units at Austurfjöll
574 may have been fissure-fed, including the pillow lava sheets. These fissure vents were widely
575 distributed over the 48 km^2 area now covered by the Austurfjöll massif (Figure 8). Eruptive units
576 have wide lateral distribution indicating that multiple vents were active during each eruptive
577 phase (Figure 10).
578 Austurfjöll contains deposits that predominantly record the interaction of magma with
579 water, with a notable transition from effusive pillow lava sheets to explosive tindar forming
580 activity (Table 4). The onset of explosive activity during an ice-confined eruption can be the
581 result of a change in internal eruptive conditions or external environmental conditions, or a
582 combination of the two. Internal conditions include eruptive mass discharge rate, gas content, or
583 crystal content. External conditions include an increase of infiltration of water into a vent, or
584 depressurization as a result in the elevation gain of the eruptive vent and/or a decrease in the
585 level of the confining water due to drainage. Evidence for a combination of triggering
586 mechanisms can be found in textural signatures of the primary deposits lapilli and ash tuffs (Lt1,
587 At1, Lt2, and At2). Detailed investigation of the Lt1 facies revealed that both magmatic and
588 phreatomagmatic activity contributed to the production of fragmental material at Austurfjöll. In
589 particular, an increase in mass discharge rate in an aqueous environment with a changing water
590 level triggered local transitions from effusive to explosive activity (Graettinger et al. 2013b).
591 Similarly, the common transition from regular pillowed lavas (Pl1) to irregular pillowed lavas
592 (Pl2) indicates that subtle variations in the eruptive flux were common during the formation of
593 pillow lava sheets that dominate Units 2 and 3.
594 At the same time, local textural variations indicate the eruptive environment was variable
595 during the construction of Austurfjöll. Large channels (100 m in diameter) cross-cut Unit 2

primary and remobilized lapilli tuffs, and are filled with bedded ash tuffs. Such channels indicate that drainage of large volumes of water occurred while fragmental materials were unconsolidated, and channels were filled by multiple pulses and / or discrete sediment gravity flows (Figure 7b). Stratigraphically younger units at high elevations, such as Unit 6 (1160 m asl), preserve localized subaqueous effusive-only activity. Pillow fragments in the breccias found along the caldera rim (>1200 m asl) suggest ice-confined lake levels higher than the current top of the massif. Additionally, small outcrops of subaerial lavas (Unit 2 and Unit 3) are found interbedded and transitioning into pillowed lavas, and indicate an increase in water level during the construction of the massif. This suggests that the growth of Austurfjöll as a whole was influenced by a mechanism that produced a near permanent shift from effusive to explosive activity, with variations in the lake level that produced local emergence and flooding. As the initial effusion-dominated pillow lava sheets result in an overall increase in elevation of 100 m and, therefore, a decrease in the potential water column over the eruptive vents, the simplest solution for massif-wide eruption behavioral changes is for the depressurization associated with the decreased water depth to enable the transition to explosive activity. This growth trend was accompanied by drainage events, fluctuations in eruptive flux, and continued melting of the confining ice sheet.

The lithofacies distribution and deposit textures enable inferences about the configuration of ice and meltwater lakes during the construction of Austurfjöll. The presence of vertical pillow lavas (Unit 2) and radial cooling cracks in non-pillowed lavas (Unit 6) indicate that the confining ice was proximal to the growing massif. Diamictite deposits between Unit 2 and Unit 3 indicate that this ice locally re-advanced onto the massif and eroded lavas between eruptive units. Additionally, localized subaerial deposits, or subaerial components in clastic units (i.e. Lt3) reflect variable water levels during the construction of Austurfjöll, likely related to drainage and refilling of the ice-confined lake level.These features suggest that there was not a single stable lake present at Austurfjöll during construction. More likely, the growth Austurfjöll was associated with the formation of numerous ephemeral meltwater lakes impacted by variable configurations of confining ice and eruptive activity (Figure 11). The transitions between subaerial and subaqueous lithofacies at Austurfjöll are highly localized, unlike extensive passage zones described tuya and tindar constructs in Iceland and British Columbia (Werner et al. 1996; Skilling et al. 2009; Russell et al. 2013) and Antarctica (Smellie et al. 2013), and reflect not only a variable lake level, but restricted bodies of meltwater as well as extensive massif covering lakes. The extent of these lakes were likely influenced by the area of the active vent over time, as there is no evidence of a long term established passage zone across the massif at

any elevation. Historical observations of vent proximal ice during the 1996 Gjalp eruption indicated that the ice responded rapidly to the presence, and absence of ongoing eruptive activity (Gudmundsson et al. 1997). The extent of the pillow lava sheets indicate that there may have been a fairly large body of ice-confined meltwater early in the history of Austurfjöll, while smaller eruptive units, and individual tindars, may reflect limited bodies of meltwater between Austurfjöll and the confining ice mass. The thickness of the sequence and the absence of significant subaerial facies reflect the thickness of ice present during the construction of the massif (ca. 700-900 m), which agrees with its position near the center of the modeled Weichselian ice sheet (Hubbard et al. 2006).

Multi-vent fissure-fed glaciovolcanic massif

The multi-vent construction of Austurfjöll contrasts with the morphology of more familiar tuyas and tindars. Tuyas have focused or centralized vent locations as in Herðubreið (Werner et al. 1996, Werner and Schmincke 1999), and Hlöðufell (Skilling 2009) in Iceland and Hoodoo Mountain (Edwards et al. 2002), Mathew's Tuya (Edwards et al. 2011) and Kima' Kho (Ryane et al. 2011) in British Columbia Canada. Each case is marked by distinctive lithofacies such as a subaerial lava cap with lava deltas (that can define a passage zone), that reflect prolonged subaerial activity (Skilling 1994, 2009; Werner and Schmincke 1999; Smellie et al. 2008; Russell et al. 2013). There is no preserved evidence of prolonged subaerial activity at Austurfjöll.

Tindars are linear features constructed from vents aligned along an eruptive fissure, and each tindar is considered to be the product of one eruptive episode, like at Helgafell (Schopka et al. 2006), Sveifluhals (Mercurio 2011), and Undirhlíðar (Pollock et al. 2014) in Iceland. The tindars at Austurfjöll are broadly similar to tindars described elsewhere (Mercurio 2011), with an important difference at Austurfjöll being the close proximity, and overlapping, of a large number of tindars. Additionally, the pillow lava sheets and the pillow mounds at Austurfjöll have not been observed in similar abundance at either tuyas or tindars. Much larger pillow mounds have been described in British Columbia (Canada) by Hickson (2000) as independent edifices with diameters up to 2 km, in contrast to the decimeter examples at Austurfjöll. This size discrepancy reflects the influence of the multi-vent, fissure-dominated construction of Austurfjöll.

The overall structure of Austurfjöll has little in common with tuyas but much in common with tindars, reflecting a new mechanism for glaciovolcanic massif construction via multiple tindars as a part of a long-lived central volcano. The westernmost sector of the Austurfjöll glaciovolcanic massif has been removed by two caldera collapses, one in 1875 AD, and an earlier collapse of unknown age. Additional glaciovolcanic massifs at Askja are present in the

North East and Thorvaldstindur along the southern margin of the current lake. The overall complex presents a unique morphology that has yet to be considered in planetary searches for glaciovolcanic constructs (e.g. Ghatan and Head 2002; Houvis et al. 2008; Martinez-Alonso et al. 2011).

The architecture of Austurfjöll indicates that it was constructed via multiple glaciovolcanic eruptions of modest volume. The Weichselian activity has a strong parallel in Holocene volcanism at Askja, where similar activity (i.e. fissure eruptions of modest volume) has persisted from the early Holocene to the present day (Annertz 1985; Höskuldsson 1987; Sigvaldason et al. 1992; Kuritani et al. 2011; Hartley et al. 2016) the most recent eruption being in 1961 (Thorarinsson and Sigvaldason 1962). It is likely that other large basaltic volcanoes in Iceland that interacted with an ice sheet also preserve evidence of prolonged multi-vent, multi-fissure eruptions through multiple ice-confined lakes.

Conclusions

The glaciovolcanic history of Austurfjöll represents the construction of a complicated fissure-fed massif dominated by pillow lava sheets and numerous (>40) overlapping tindars in several ice-confined lakes, during the last (Weichselian) glacial period. This study represents the first description of a disperse multi-vent glaciovolcanic massif forming part of long-lived basaltic volcano in Iceland. The glaciovolcanic activity of Austurfjöll contributed a significant volume of basaltic material to Askja volcano through the formation of pillow lava sheets and overlapping tindars with seven recognizable eruptive units. The lithofacies indicate that activity shifted from predominantly effusive activity of early constructional phases to explosive-dominated phases as the massif increased in elevation, and was subject to temporary meltwater drainage events with local increases in eruptive flux. Austurfjöll expands our understanding of the longevity and chemical variability at Icelandic basaltic volcanoes, and the effects on ice sheets present at the time of eruption. In particular, Austurfjöll represents the first example of a complicated and widely dispersed vent system that resulted in a newly described morphology and constructional history relative to previously described glaciovolcanic systems in Iceland, and around the world. This broader distribution of vents, in contrast to more centralized tuyas has important implications for the influence of a long-lived basaltic volcano on the overlying ice sheet and the generation of multiple variable meltwater lakes. This new glaciovolcanic geometry should be considered in the future identification of glaciovolcanic massifs on Earth and Mars. However, if the structure is realized to be unique to Askja, it raises important questions about

the tectonic setting of central Iceland and the influence of the hotspot, or perhaps the role of other eruptions, including caldera forming events, on the structure of Askja volcano.

Acknowledgments

This work was made possible by a National Science Foundation grant to IPS, DMcG, and AH (Award number 0910526). Our gratitude goes to Haskolí Islands, NORVOLK, and the Vatnajökull National Park, for field logistics and permits. Field assistance from Robin Wham, Rachel Lee, Antonia Lema, Kevin Reath, and Mary Kate Ellis was invaluable. Comments by K. Russell, an anonymous reviewer, and the editors greatly improved the manuscript.

References

Annertz K, Nilsson M, Sigvaldason GE (1985) The postglacial history of Dyngjufjöll In: NORVULK. Nordic Volcanological Institute, Reykjavik p22

Baer G (1995) Fracture propagation and magma flow in segmented dykes: Field evidence and fabric analyses, Makhtesh Ramon, Israel. In: Baer G, Heimann A (eds) Physics and Chemistry of Dykes. Geological Survey of Israel, Balkema pp 125-140

Bennett MR, Huddart D, Waller RI (2006) Diamict fans in subglacial water-filled cavities- a new glacial environment. Quaternary Science Reviews 25:3050-3069, doi:10.1016/j.quascirev.2006.05.004

Bergh SG, Sigvaldason GE (1991) Pleistocene mass-flow deposits of basaltic hyaloclastite on a shallow submarine shelf, South Iceland. Bulletin of Volcanology 53:597-611

Carey R, Houghton BF, Thordarson T (2009) Abrupt shifts between wet and dry phases of the 1875 eruption of Askja Volcano: Microscopic evidence for macroscopic dynamics. Journal of Volcanology and Geothermal Research 184:256-270. doi: 10.1016/j.jvolgeores.2009.04.003

Carlisle D, (1963) Pillow breccias and their aquagene tuffs, Quadra Island, British Columbia. The Journal of Geology 71: 48-71.

Carrivick JL, Russell AJ, Rushmer EL, Tweed FS, Marren PM, Deeming H, Lowe OJ (2009) Geomorphological evidence towards a de-glacial control on volcanism. Earth Surface Processes and Landforms 34:1164-1178, doi:10.1002/esp.1811

Dimroth E, Pierre C, Leduc M, Sanshagrin Y (1978) Structure and organization of Archean subaqueous basalt flows, Rouyn-Noranda area, Quebec, Canada. Canadian Journal of Earth Science 15:902-918

729 Doyle MG (2000) Clast shape and textural associations in peperite as a guide to hydromagmatic
730 interactions: Upper Permian basaltic and basaltic andesite examples from Kiama, Australia.
731 Australian Journal of Earth Sciences 47:167-177, doi:10.1046/j.1440-0952.2000.00773.x

732 Edwards BR, Russell JK, Anderson RG (2002) Subglacial, phonolitic volcanism at Hoodoo
733 Mountain volcano, northern Canadian Cordillera. Bulletin of Volcanology 64:254-272,
734 doi:10.1007/s00445-002-0202-9

735 Edwards BR, Skilling, IP, Cameron B, Haynes C, Lloyd A, Hungerford JHD (2009) Evolution of
736 an englacial volcanic ridge: Pillow Ridge tindar, Mount Edziza volcanic complex, NCVP, British
737 Columbia, Canada. Journal of Volcanology and Geothermal Research 185:251-275,
738 doi:10.1016/j.jvolgeores.2008.11.015

739 Edwards BR, Russell JK, Simpson K (2011) Volcanology and petrology of Mathews Tuya,
740 northern British Columbia, Canada: glaciovolcanic constraints on interpretations of the 0.730 Ma
741 Cordilleran paleoclimate. Bulletin of Volcanology 73:479-496, doi:10.1007/s00445-010-0418-z

742 Edwards BR, Gudmundsson MT, Russell JK (2015) Glaciovolcanism. In: Sigurdsson H (eds)
743 The Encyclopedia of Volcanoes, 2nd Edition. Academic Press, pp 377-393, doi:10.1016/B978-
744 0-12-385938-9.00020-1

745 Einarsson P (2008) Plate boundaries, rifts and transforms in Iceland. Jokull 58: 35-58.

746 Ghatan G, Head JW (2002) Candidate subglacial volcanoes in the south polar region of Mars:
747 Morphology, morphometry, and eruption conditions 107: 2-1-1-19. doi: 10.1029/2001JE001519

748 Goto Y, McPhie J (2004) Morphology and propagation styles of Miocene submarine basanite
749 lavas at Stanley, northwestern Tasmania, Australia. Journal of Volcanology and Geothermal
750 Research 130:307-328, doi:10.1016/S0377-0273(03)00311-1

751 Graettinger AH, Skilling IP, McGarvie DW, Höskuldsson A (2012) Intrusion of basalt into frozen
752 sediments and generation of Coherent-Margined Volcaniclastic Dikes (CMVDs). Journal of
753 Volcanology and Geothermal Research 217-218:30-38, doi:10.1016/j.jvolgeores.2011.12.008

754 Graettinger AH, Ellis MK, Skilling IP, Reath K, Ramsey MS, Lee RJ, Hughes CG, McGarvie DW
755 (2013a) Remote sensing and geologic mapping of glaciovolcanic deposits in the region
756 surrounding Askja (Dyngjufjöll) volcano, Iceland. International Journal of Remote Sensing
757 34:7178-7198, doi:10.1080/01431161.2013.817716

758 Graettinger AH, Skilling IP, McGarvie DW, Höskuldsson A (2013b) Subaqueous basaltic
759 magmatic explosions trigger phreatomagmatism: a case study from Askja, Iceland. Journal of
760 Volcanology and Geothermal Research 264:17-35, doi:10.1016/j.jvolgeores.2013.08.001

761 Gregg TKP, Fink JH (1995) Quantification of submarine lava-flow morphology through analog
762 experiments. Geology 23:73-76

763 Gregg TKP, Smith D (2003) Volcanic investigations of the Puna Ridge, Hawai'i: relations of lava
764 flow morphologies and underlying slopes. Journal of Volcanology and Geothermal Research
765 126:63-77, doi:10.1016/S0377-0273(03)00116-1

766 Gudmundsson MT, Sigmundsson F, Björnsson H (1997) Ice-volcano interaction of the 1996
767 Gjálp subglacial eruption, Vatnajökull, Iceland. Nature 389:954-957

768 Hartley ME, Thordarsson T, de Joux A (2016) Postglacial eruptive history of the Askja region,
769 North Iceland. Bulletin of Volcanology 78:28 doi: 10.1007/s00445-016-1022-7

770 Hickson CJ (2000) Physical controls and resulting morphological forms of Quaternary ice-
771 contact volcanoes in western Canada. Geomorphology 32:239-261

772 Höskuldsson Á (1987) Some chemical properties of the Askja volcanic center In: Nordic
773 Volcanological Institute, University of Iceland Reykjavík

774 Höskuldsson Á, Sparks RSJ, Carrol MR (2006) Constraints on the dynamics of subglacial basalt
775 eruptions from geological and geochemical observations at Kverkfjöll, NE-Iceland. Bulletin of
776 Volcanology 68:689-701, doi:10.1007/s00445-005-0043-4

777 Hungerford JDG, Edwards BR, Skilling IP, Cameron BI (2014) Evolution of a subglacial basaltic
778 lava flow field: Tennena volcanic center, Mount Edziza volcanic complex, British Columbia,
779 Canada. Journal of Volcanology and Geothermal Research 272:39-58,
780 doi:10.1016/j.jvolgeores.2013.09.012

781 Houvis N, Lea-Cox A, Turowski JM (2008) Recent volcano-ice interaction and outburst flooding
782 in a Mars polar cap re-entrant. Icarus 197:23-38. doi: 10.1016/j.icarus.2008.04.020

783 Jakobsson SP, Gudmundsson MT (2008) Subglacial and intraglacial volcanic formations in
784 Iceland. Jökull 58:179-196

785 Jonasson K (1994) Rhyolite volcanism in the Krafla central volcano, north-east Iceland. Bulletin
786 of Volcanology 56: 516-528.

787 Kennish MJ, Lutz RL (1998) Morphology and distribution of lava flows on mid-ocean ridges: a
788 review. Earth-Science Reviews 43:63-90, doi:10.1016/j.geomorph.2006.12.002

789 Komatsu G, Arzhannikov SG, Arzhannikova AV, Ershov K (2007) Geomorphology of subglacial
790 volcanoes in the Azas Plateau, the Tuva Republic Russia. Geomorphology 888:312-328

791 Kralj P (2012) Facies architecture of the Upper Oligocene submarine Smrekovec stratovolcano,
792 Northern Slovenia. Journal of Volcanology and Geothermal Research 247-248:122-138,
793 doi:10.1016/j.jvolgeores.2012.07.016

794 Kuritani T, Yokoyama T, Kitagawa H, Kobayashi K, Nakamura E (2011) Geochemical evolution
795 of historical lavas from Askja Volcano, Iceland: Implications for mechanisms and timescales of
796 magmatic differentiation. Geochemica et Cosmochimica Acta 75:570-587,
797 doi:10.1016/j.gca.2010.10.009

798 Lacasse C, Sigurdsson H, Carey SN, Johannesson H, Thomas LE, Rogers NW (2007) Bimodal
799 volcanism at the Katla subglacial caldera, Iceland: insight into the geochemistry and
800 petrogenesis of rhyolitic magmas. Bulletin of Volcanology 69:373. doi: 10.1007/s00445-006-
801 0082-5

802 Loughlin SC (2002) Facies analysis of proximal subglacial and proglacial volcaniclastic
803 successions at the Eyjafjallajökull. In: Smellie JL, Chapman MG (ed) Volcano-Ice Interaction on
804 Earth and Mars. The Geological Society of London, London, pp 149-178

805 Macdonald R, Sparks R, Sigurdsson H, Mattey D, McGarvie D, Smith R (1987) The 1875
806 eruption of Askja volcano, Iceland: Combined fractional crystallization and selective
807 contamination in the generation of rhyolitic magma. Mineralogical Magazine 51: 183-202.
808 doi:10.1180/minmag.1987.051.360.01

809 Maicher D, White JDL, Batiza R (2000) Sheet hyaloclastite: density-current deposits of quench
810 and bubble-burst fragments from thin, glassy sheet lava flows, Seamount Six, Eastern Pacific
811 Ocean. Marine Geology 171:75-94, doi:10.1016/S0025-3227(00)00109-2

812 Martinez-Alonso S, Mellon MT, Banks MA, Keszthelyi LP, McEwen AS, The HiRISE Team
813 (2011) Evidence of volcanic and glacial activity in Chryse and Acidalia Planitiae, Mars. Icarus
814 212: 597-621. doi: 10.1016/j.icarus.2011.01.004

815 McPhie J, Doyle MG, Allen CC (1993) Volcanic Textures: A guide to the interpretation of
816 textures in volcanic rocks. CODES Key Centre, University of Tasmania Hobart p. 198

817 Mercurio E (2011) Processes, products and depositional environments of ice-confined basaltic
818 fissure eruptions: a case study of the Sveifluhals volcanic complex, SW Iceland. Unpublished
819 dissertation. Department of Geology and Planetary Science, University of Pittsburgh

820 Parfitt EA, Gregg TKP, Smith D (2002) A comparison between subaerial and submarine
821 eruptions at Kilauea Volcano, Hawaii: implications for the thermal viability of lateral feeder dikes.
822 Journal of Volcanology and Geothermal Research 113:213-242, doi:10.1016/S0377-
823 0273(01)00259-1

824 Pollock M, Edwards BR, Hauksdottir S, Alcorn R, Bowman L (2014) Geochemical and
825 lithostratigraphic constrains on the formation of pillow-dominated tindars from Undirhlíðar
826 quarry, Reykjanes Peninsula, southwest Iceland. Lithos 200-201:314-333,
827 doi:10.1016/j.lithos.2014.04.023

828 Ryane C, Edwards BR, Russell JK (2011) The volcanic stratigraphy of Kima'Kho Mountain: A
829 Pleistocene tuya, northwestern British Columbia. In: Geological Survey of Canada Current
830 Research. Geological Survey of Canada, doi:10.4095/289196

831 Rivalta E, Dahm T (2006) Acceleration of buoyancy-driven fractures and magmatic dikes
832 beneath the free surface. Geophysical Journal International 166:1424-1439, doi:10.1111/j.1365-
833 246X.2006.02962.x

834 Russell JK, Edwards BR, Porritt LA (2013) Pyroclastic passage zones in glaciovolcanic
835 sequences. Nature 4 doi:10.1038/ncomms2829

836 Russell JK, Edwards BR, Porritt LA, Ryane C (2014) Tuyas: a descriptive genetic classification.
837 Quaternary Science Reviews 87:70-81, doi:10.1016/j.quascirev.2014.01.001

838 Sansone FJ, Smith JR (2006) Rapid mass wasting following nearshore submarine volcanism on
839 Kilauea volcano, Hawaii. Journal of Volcanology and Geothermal Research 151:133-139,
840 doi:10.1016/j.jvolgeores.2005.07.026

841 Schopka HH, Gudmundsson MT, Tuffen H (2006) The formation of Helgafell, southwest Iceland,
842 a monogenetic subglacial hyaloclastite ridge: Sedimentology, hydrology and volcano-ice
843 interaction. Journal of Volcanology and Geothermal Research 152:359-377,
844 doi:10.1016/j.jvolgeores.2005.11.010

845 Sigvaldason GE (1968) Structure and products of subaquatic volcanoes in Iceland.
846 Contributions to Mineralogy and Petrology 18:1-16

847 Sigvaldason GE, Annertz K, Nilsson M (1992) Effect of glacier loading/deloading on volcanism:
848 postglacial volcanic production rate of the Dyngjufjöll. Bulletin of Volcanology 54:385-392

849 Skilling IP (1994) Evolution of an englacial volcano: Brown Bluff, Antarctica. Bulletin of
850 Volcanology 56:573-591

851 Skilling IP (2009) Subglacial to emergent basaltic volcanism at Hlöðufell, south-west Iceland: A
852 history of ice-confinement. Journal of Volcanology and Geothermal Research 185:276-289,
853 doi:10.1016/j.jvolgeores.2009.05.023

854 Skilling IP, White JDL, McPhie J (2002) Peperite: a review of magma-sediment mingling.
855 Journal of Volcanology and Geothermal Research 114:1-17, doi:10.1016/S0377-
856 0273(01)00278-5

857 Smellie JL (2006) The relative importance of supraglacial versus subglacial meltwater escape in
858 basaltic subglacial tuya eruptions: An important unresolved conundrum. Earth-Science Review
859 74:241-268 doi:10.1016/j.earscirev.2005.09.004

860 Smellie JL, Johnson JS, McIntosh WC, Esser R, Gudmundsson MT, Hambrey MJ, van Wyk de
861 Vries B (2008) Six million years of glacial history recorded in volcanic lithofacies of the James
862 Ross Island Volcanic Group, Antarctic Peninsula. Palaeogeography, Palaeoclimatology,
863 Palaeoecology 260:122-148. doi:10.1016/j.palaeo.2007.08.011

864 Smellie JL (2008) Basaltic subglacial sheet-like sequences: Evidence for two types with different
865 implications for the inferred thickness of associated ice. Earth-Science Reviews 88:60-88,
866 doi:10.1016/j.earscirev.2008.01.004

867 Smellie JL, Hole MJ (1997) Products and processes in Pliocene-Recent, subaqueous to
868 emergent volcanism in the Antarctic Peninsula: examples of englacial Surtseyan volcano
869 construction. Bulletin of Volcanology 58:628-646

870 Stevenson JA, Smellie JL, McGarvie DW, Gilbert JS, Cameron BI (2009) Subglacial
871 intermediate volcanism at Kerlingarfjöll, Iceland: magma-water interactions beneath thick ice.
872 Journal of Volcanology and Geothermal Research 185: 337-351,
873 doi:10.1016.jvolgeores.2008.12.016

874 Strand K (1987) Models for the deposition and the role of external water in explosive volcanism
875 of the Dyngjufjöll Late Pleistocene-Holocene central volcano complex in North Iceland. In:
876 Nordic Volcanological Institute, University of Iceland Reykjavik

877 Stroncik N, Schmincke H-U (2002) Palagonite- a review. International Journal of Earch Science
878 (Geol Rundsch) 91:680-697, DOI 10.1007/s00531-001-0238-7

879 Thorarinsson S, Sigvaldason G (1962) The eruption in Askja, 1961 a preliminary report.
880 American Journal of Science 260:641-651

881 Tucker DS, Scott KM (2009) Structures and facies associated with the flow of subaerial basaltic
882 lava into a deep freshwater lake: the Sulphur Creek lava flow, North Cascades, Washington.
883 Journal of Volcanology and Geothermal Research 185:311-322,
884 doi:10.1016/j.jvolgeores.2008.11.028

885 Vezzoli LM, Hauser N, Omarini R, Mazzuoli R, Acocella V (2008) Non-explosive magma-water
886 interaction in a continental setting: Miocene examples from the Eastern Cordillera. Bulletin of
887 Volcanology 71:509, doi: 10.1007/s00445-008-0239-5

888 Walker GPL (1992) Morphometric study of pillow-size spectrum among pillow lavas. Bulletin of
889 Volcanology 54:459-474

890 Watton TJ, Jerram DA, Thordarson T, Davies RJ (2013) Three-dimensional lithofacies
891 variations in hyaloclastite deposits Journal of Volcanology and Geothermal Research 250:19-
892 33, doi:10.1016/j.jvolgeores.2012.10.011

893 Werner R, Schmincke H-U, Sigvaldason GE (1996) A new model for the evolution of table
894 mountains: volcanological and petrological evidence from Herdubreid and Herdubreidartögl
895 volcanoes (Iceland) Geol Rundsch 85:390-397

896 Werner R, Schmincke H-U (1999) Englacial vs lacustrine origin of volcanic table mountains:
897 evidence from Iceland. Bulletin of Volcanology 60:335-354

898 White JDL (1996) Pre-emergent construction of a lacustrine basaltic volcano, Pahvant Butte,
899 Utah (USA). Bulletin of Volcanology 58:249-262

900 White JDL (2000) Subaqueous eruption-fed density currents and their deposits. Precambrain
901 Research 101:87-109, doi:10.1016/S0301-9268(99)00096-0

902 White JDL, McPhie J, Skilling IP (2000) Peperite: a useful genetic term. Bulletin of Volcanology
903 62:65-66

Wood DA (1976) Spatial and temporal variation in the trace element geochemistry of the eastern Iceland flood basalt succession. Journal of Geophysical Research 81(23):4353-4360

Wood DA (1978) Major and Trace Element Variations in the Tertiary Lavas of Eastern Iceland and their Significance with respect to the Iceland Geochemical Anomaly. Journal of Petrology 19(3):393-436

Figure Captions

Fig. 1 A) Map of Iceland and study area, Askja. Major volcanic zones in Iceland are highlighted, with inset of Askja volcano and Austurfjöll massif. Yellow dots indicate logs from this study, black triangles are logs collected by K. Strand and A. Höskuldsson in 1980 for NORVOLK (Strand 1987). B) Lithofacies map of Austurfjöll (outlined in black). Other regions studied using reconnaissance survey with aerial photo support. A rhyolite dome was observed in the field but not studied in detail.

Fig. 2 Example images of breccia and diamictite deposits from Austurfjöll glaciovolcanic massif. A) Pillow breccia (B1), where pillow forms are preserved (yellow circle around a 20 cm diameter pillow fragment), B) Angular block breccia (B2) with person for scale, C) Diamictite (Dia1) containing large striated rounded glacial clasts in a fine matrix units on scale are 10 cm, D) Glacial outwash (Dia2) sandy diamictite containing small rounded pebbles, arrow in scale is 10 cm.

Fig. 3 Examples of lapilli tuff deposits: A) Angular lapilli tuff (Lt1) contains glassy angular clasts that may have convolute vesicles and fluidal clast shapes (yellow line around example of fluidal clast), 1 cm increments on scale bar, B) Subrounded lapilli tuff (Lt2) contains isolated outsized clasts in a matrix of subrounded lapilli, small divisions on scale are 1 cm, C) Red scoria lapilli tuff (Lt3), dominated by subaerial components such as scoria and armored lapilli (arrows indicate armored lapilli), D) lapilli heterolithic lapilli tuff (Lt4) containing diverse subrounded clasts of subaqueous and subaerial components (arrows indicate different clast types R= oxidized subaerial lava, D= dense basalt, Bx = porphyritic basalt).

Fig. 4 Examples of ash-dominated tuff A) massive ash tuff (At1) is poorly sorted coarse ash with occasional outsized clasts (blocks). Bedded lapilli tuff (At2) contains well sorted layers of coarse to fine ash (B, D) displayed bedding on the centimeter to decimeter scale with rare loading structures (B yellow arrows indicate loading structures, 10 cm increments on scale bar). C) Alternating bedded ash tuff (At3) displays variations in bedding and grain size on the decimeters with occasional sedimentary structures such as cross-bedding, or ripples.

Fig. 5 Deformed domains of ash tuff (At4) are common around the massif overlying fragmental deposits from breccias to tuffs. The domains contain internal sedimentary structures with individual beds displaying variable sorting. The domains display dramatic folding and centimeter scale convolutions. The domains have dips along fold axes as high as 85 degrees. Yellow lines follow example bedding planes to highlight the intense folding. Scale bar has 10 cm increments.

Fig. 6 Example stratigraphic logs from Austurfjöll. Section locations are indicated in Figure 1. Lithofacies in these sections represent common associations between facies types, but cannot be traced across the massif as the structure is divided by smaller constructional features (see Supplementary material). Assignment to eruptive units is described in Geochemistry section.

Fig. 7 Examples of major features at Austurfjöll massif. A) Isolated tindars with visible intrusive core, view to southeast towards Vatnajökull. B) Eroded channel ~ 100 m wide in Astronaut Gully

looking towards Herðubreið. C) Pillow lava sheets (60-100 m thick) are composed of pillow lavas (Pl1, Pl2) and associated breccias (B1-B2) exposed in steep sided gully on eastern edge of Austurfjöll. As shown here pillow lava sheets can be composed of multiple units that fill and level the topography. D) Pillow mounds occur in isolation up to 30 m high, and in clusters 15 m high, overlapping other glaciovolcanic deposits, yellow line indicates tops of clustered pillow mounds.

Fig. 8 Hillshade produced from a 10 m DEM of Austurfjöll Askja used to indicate location of vents (predominantly tindars) identified either through field relationships, topography or speculation (incomplete field or topographic evidence). The distribution of the more than 50 surficially exposed vents results in a unique morphology of the massif and neighboring Thorvaldstindur along the southern end of Öskjuvatn.

Fig. 9 Variation diagrams of Austurfjöll major and trace element geochemistry. Units were initially divided based on stratigraphic relationships, then samples not well constrained by stratigraphy were assigned to a Unit based on trace element geochemistry characteristics of recognized units. A) Total alkali versus silica plot. B) CaO vs. TiO. C- D) Incompatible trace elements Nb vs Y and Zr vs Rb respectively. Incompatible element enrichment trend is: Unit 6 < Unit 5< Unit 4< Unit 1< Unit 2< Unit 3< Unit 7.

Fig. 10 A) Map of eruptive units at Austurfjöll defined by stratigraphy supplemented with geochemical data. B) Insert region of map to highlight the small exposure of Unit 4. C) Simplified stratigraphic column of the history of the glaciovolcanic massif. Relative width of the column is reflective of unit distribution, while thickness corresponds to unit thickness. The appearance of macro-porphyritic units is noted. The Units that are cut by caldera faults are indicated. See Online Resource 2 for cross-sections.

Fig. 11 Simplified chronology of relative ice and meltwater positions based on lithofacies mapping and eruptive chronology for Austurfjöll massif using an W-E section. This schematic highlights the variability and recurring nature of meltwater lakes over the massif. The water and ice positions given here are minimums, values in italics are maximum elevations of subaqueous deposits for a given unit. Distributions and geometries that involve thicker ice or additional bodies of meltwater are possible. Additional drainage events (as depicted for Unit 2) are also possible. The meltwater is depicted as an open lake due to the large areal extent of the eruptive deposits (Unit 2 & 3). Question marks indicate poorly constrained ice conditions.

Online Resource 1 Complete geochemistry dataset of Askja samples.

Online Resource 2 Example cross-sections through the Austurfjöll massif indicating the development of massif as a sequence of fissure fed pillow lava sheets followed by more explosive tindars. A rhyolite dome was observed but poorly constrained.

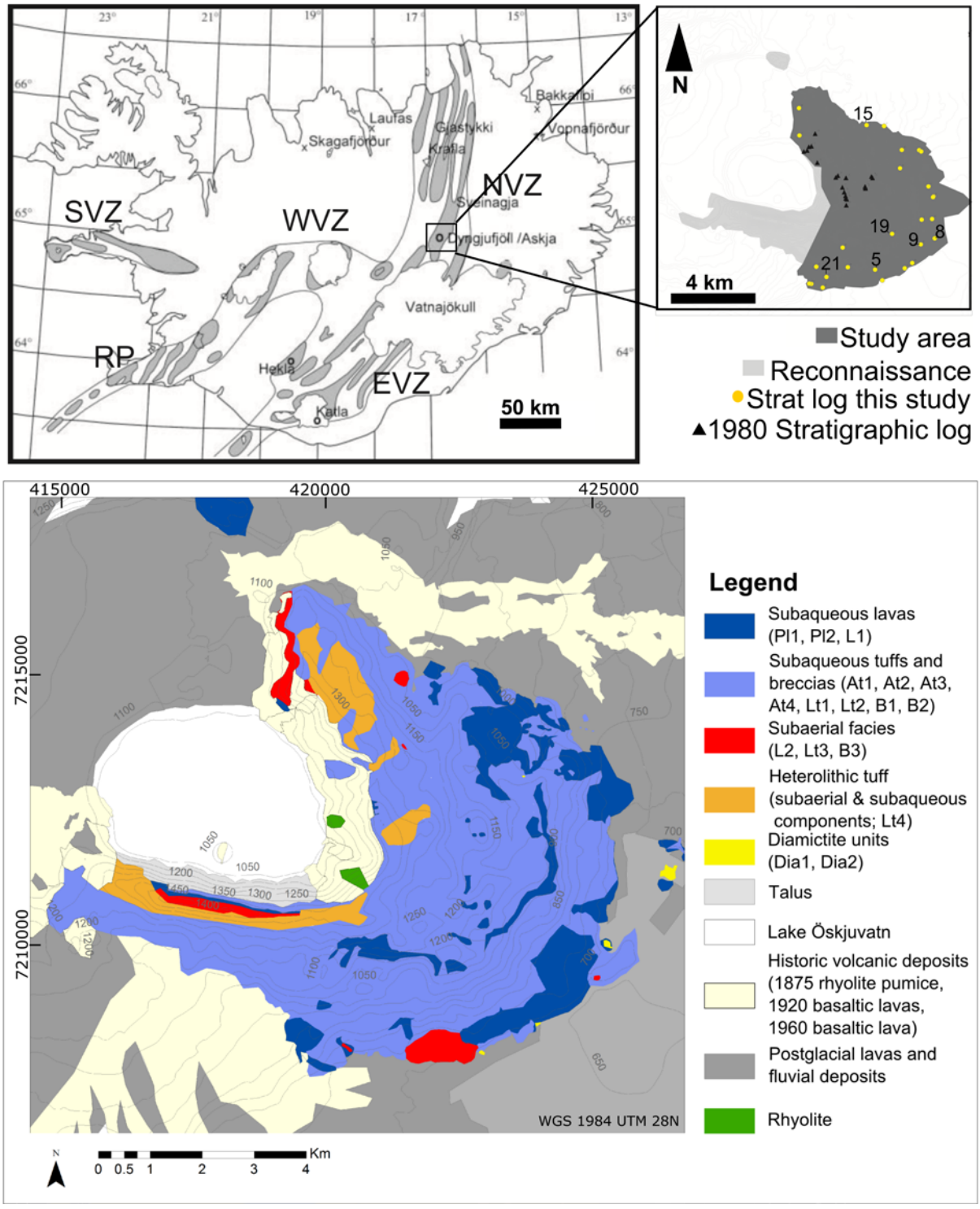

Figure 1: A) Map of Iceland and study area, Askja Iceland. Major volcanic zones in Iceland are highlighted, with inset of Askja volcano and Austurfjöll massif. Yellow dots indicate logs from this study, black triangles are logs collected by K. Strand and A. Höskuldsson in 1980 for NORVOLK (Strand 1987). Numbers for logs presented here. Light grey regions studied in less detail. B)

Simplified lithofacies map of Austurfjöll. For more detail see Graettinger et al. (2013b). Contour intervals of 50 m.

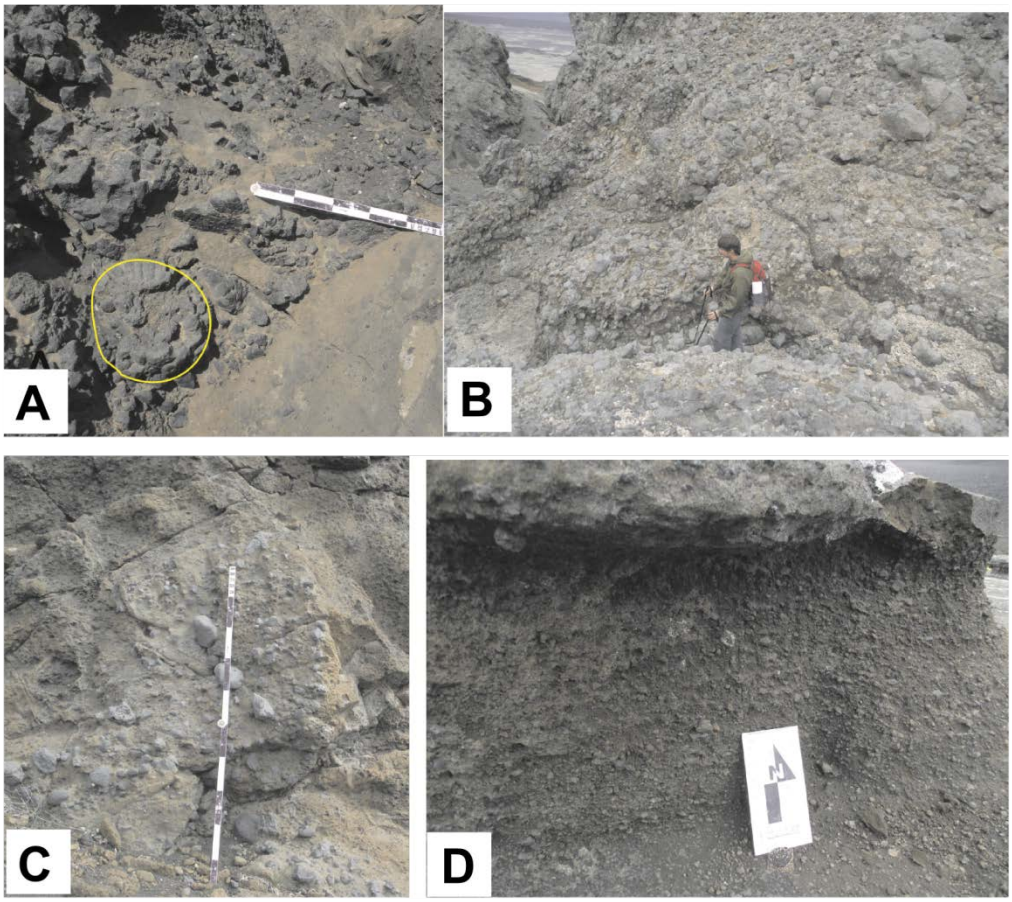

Figure 2: Example images of breccia and conglomerate deposits from Austurfjöll glaciovolcanic massif. A) Pillow breccia (B1), where pillow forms are preserved; B) Angular block breccia (B2); C) Diamictite (Dia1) containing large striated rounded glacial clasts in a fine matrix; D) Glacial outwash (Dia2) sandy conglomerate containing small rounded pebbles.

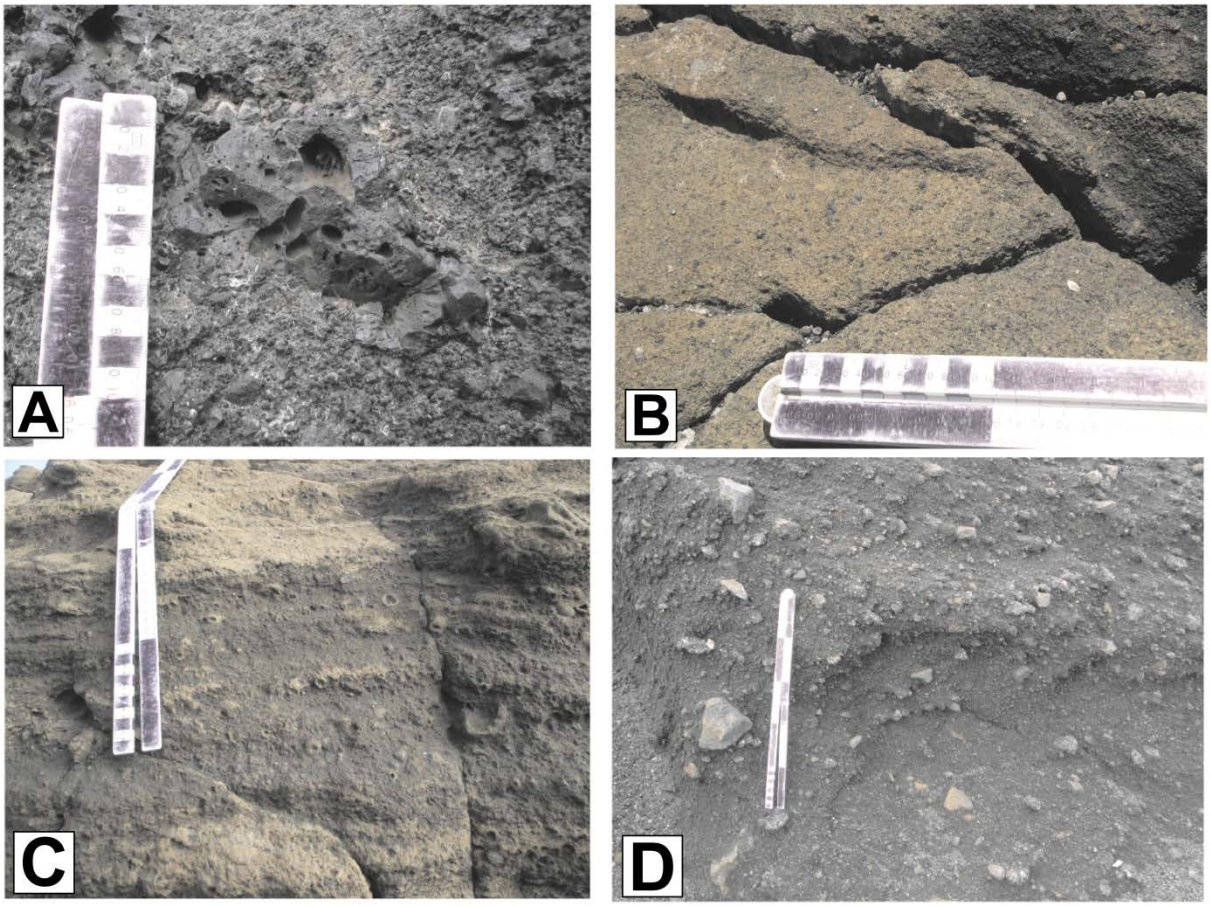

Figure 3: Examples of lapilli tuff deposits: A) Angular lapilli tuff (Lt1) contains glassy angular clasts that may have convolute vesicles and fluidal clast shapes, B) Subrounded lapilli tuff (Lt2) contains isolated outsized clasts in a matrix of subrounded lapilli, C) Red scoria lapilli tuff (Lt3), dominated by subaerial components such as scoria and armored lapilli as pictured, D) lapilli heterolithic lapilli tuff (Lt4) containing diverse subrounded clasts of subaqueous and subaerial components.

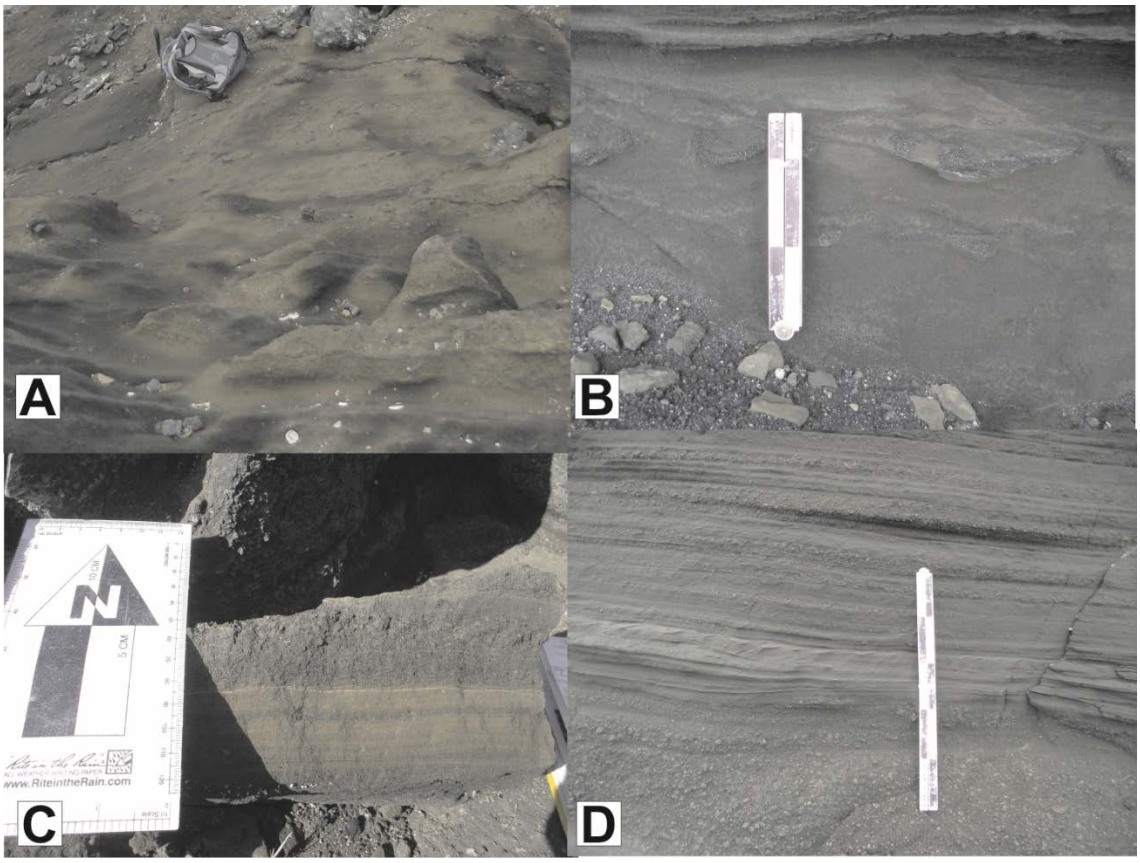

Figure 4: A) massive ash tuff (At1) is poorly sorted coarse ash with occasional outsized clasts (blocks). Bedded ash and lapilli tuff (At2) contains well sorted layers of coarse to fine ash (B, D) displayed bedding on the centimeter to decimeter scale with rare loading structures (B). C) Alternating bedded ash tuff (At3) displays variations in bedding and grain size on the decimeters with occasional sedimentary structures such as cross-bedding, or ripples.

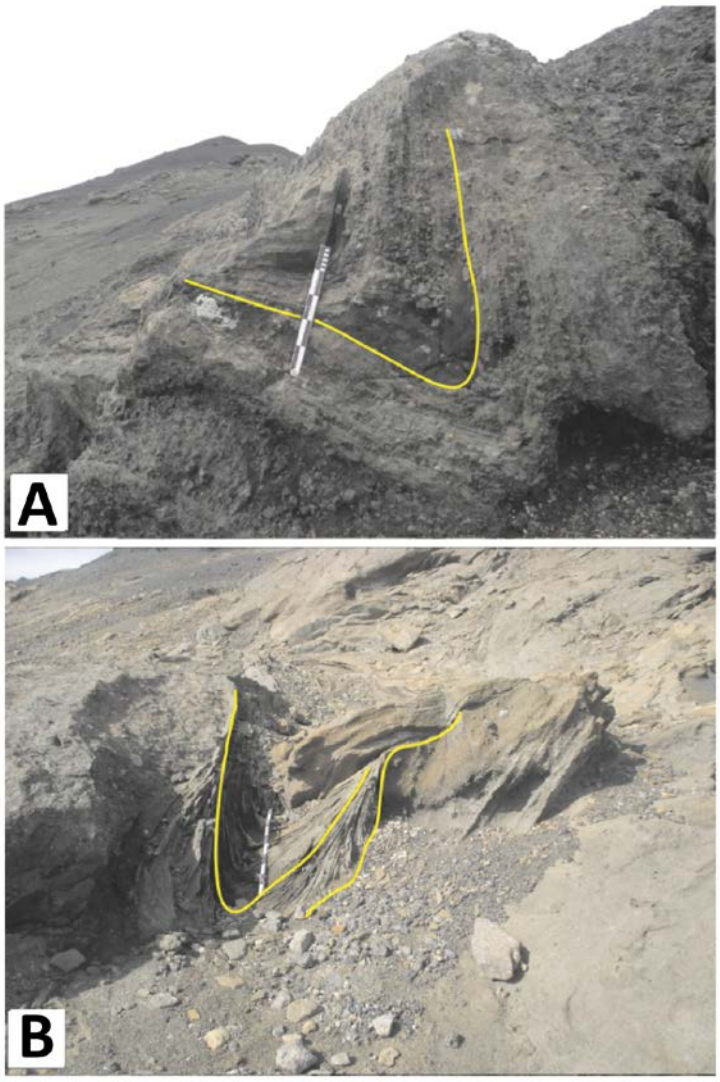

Figure 5: Deformed domains of ash tuff (At4) are common around the massif overlying fragmental units from breccias to tuffs. The domains contain internal sedimentary structures with individual beds displaying variable sorting. The domains display dramatic folding and centimeter scale convolutions. The domains have dips along fold axes as high as 85 degrees.

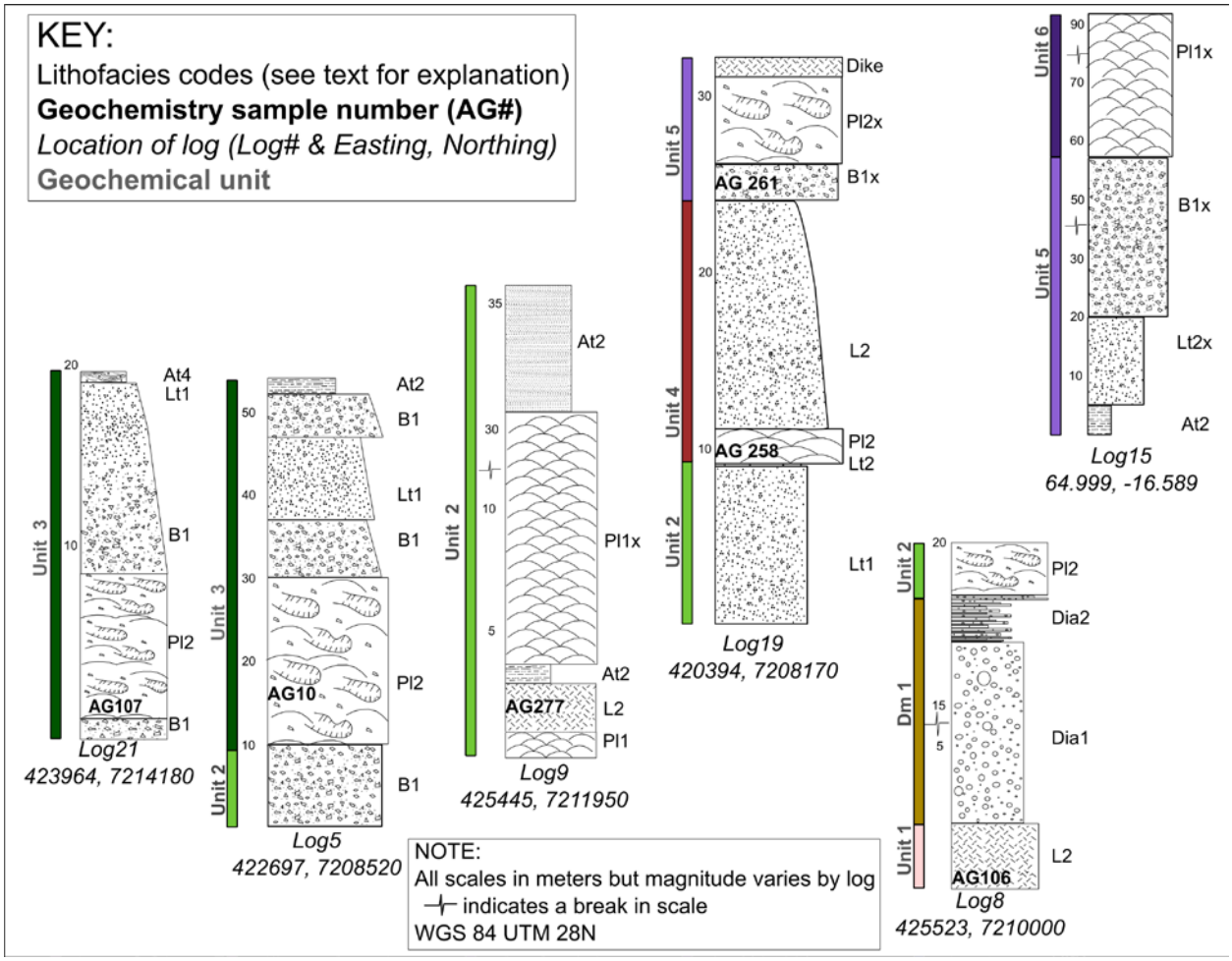

Figure 6 Example stratigraphic logs from Austurfjöll. Section locations are indicated in Figure 1. Lithofacies in these sections represent common associations between facies types, but cannot be traced across the massif as the structure is divided by smaller constructional features (see Supplementary material). Assignment to eruptive units is described in Geochemistry section.

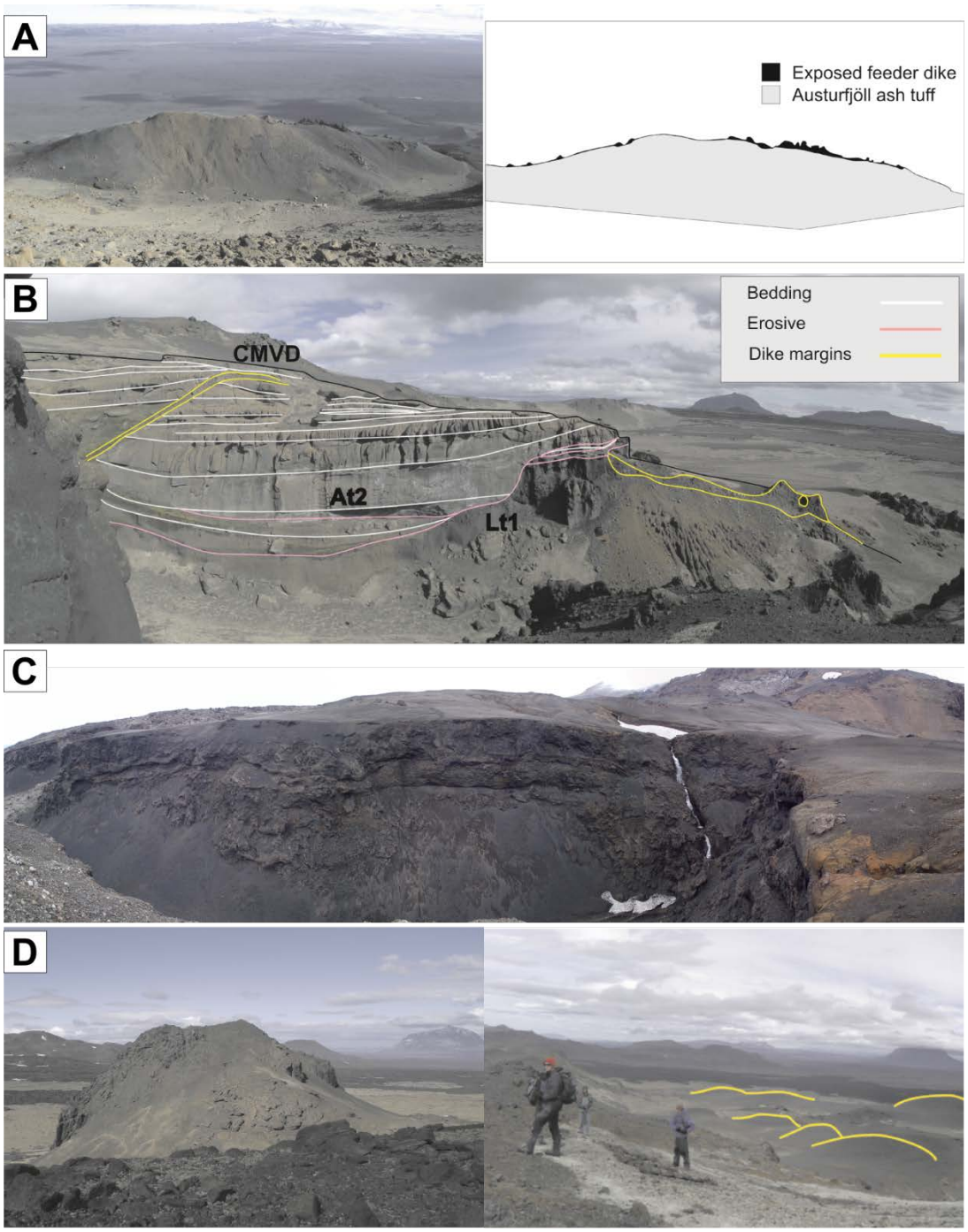

Figure 7: Examples of major features at Austurfjöll massif. A) Isolated tindars with visible intrusive core, view to southeast towards Vatnajökull. B) Eroded channel ~ 100 m wide in Astronaut Gully looking towards Herðubreið. C) Pillow lava sheets (60-100 m thick) are composed of pillow lavas (Pl1, Pl2) and associated breccias (B1-B2) exposed in steep sided gully on eastern edge of Austurfjöll. D) Pillow mounds occur in isolation up to 30 m tall and in clusters 15 m tall overlapping other glaciovolcanic deposits.

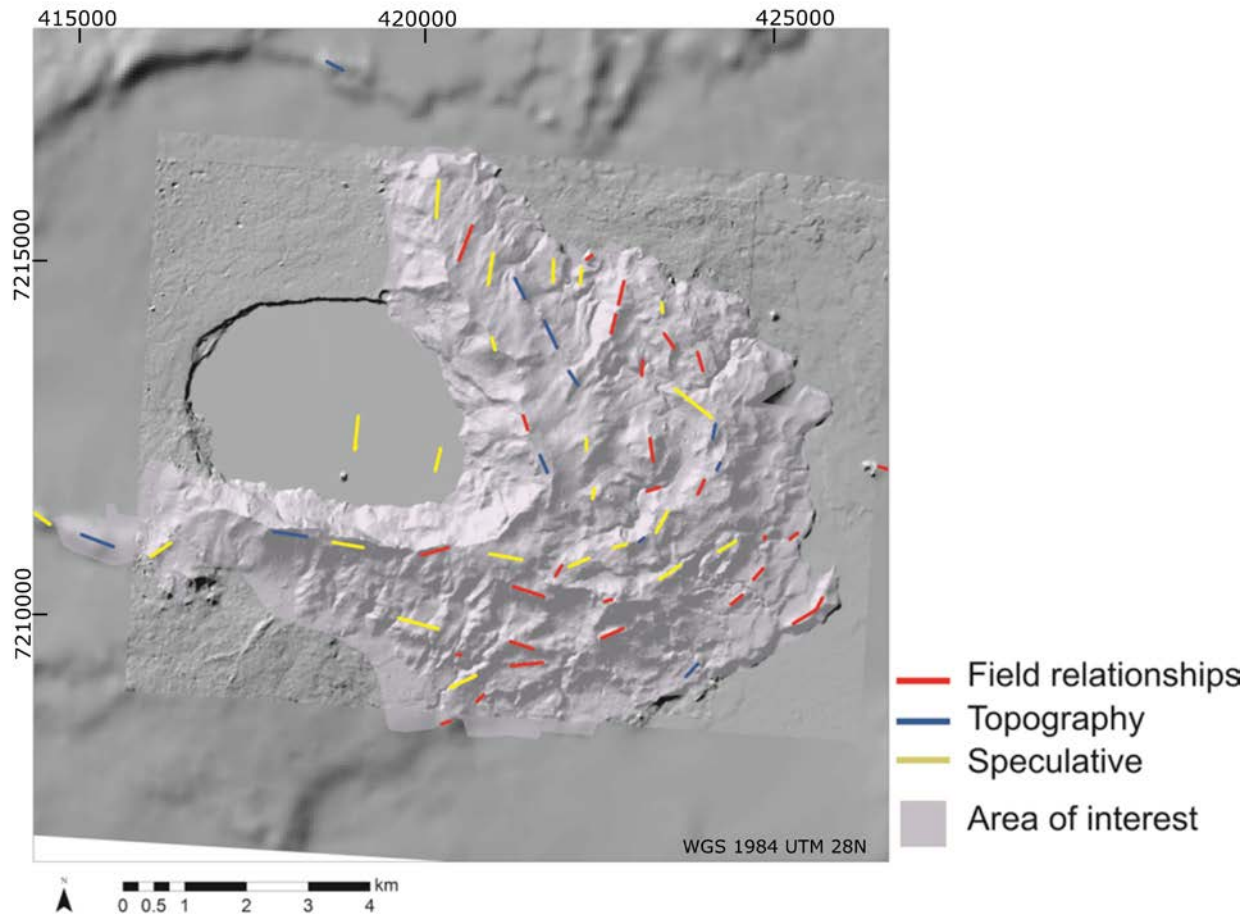

Figure 8: Hillshade produced from a 10 m DEM of Austurfjöll Askja used to indicate vents (predominantly fissure ridges) identified either through field relationships, topography or speculation (incomplete field or topographic evidence). The distribution of the more than 50 surficially exposed vents results in a unique morphology of the massif and neighboring Thorvaldstindur along the southern end of Öskjuvatn.

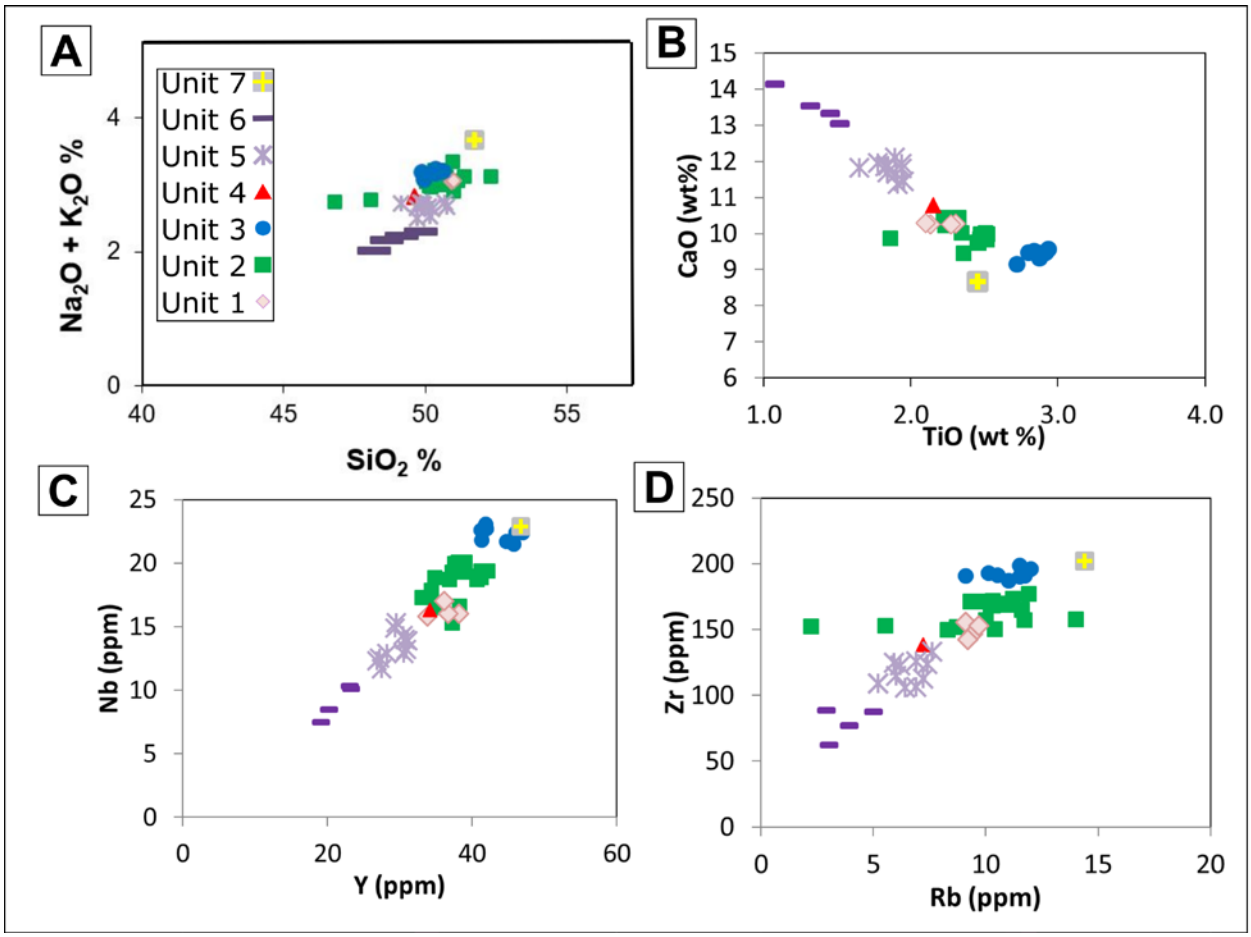

Figure 9: Variation diagrams of Austurfjöll major and trace element geochemistry. Units were initially divided based on stratigraphic relationships, then samples not well constrained by stratigraphy were assigned to a Unit based on trace element geochemistry characteristics of recognized units. A) Total alkali versus silica plot. B) CaO vs. TiO. C- D) Incompatible trace elements Nb vs Y and Zr vs Rb respectively. Incompatible element enrichment trend Unit 6 < Unit 5< Unit 4< Unit 1< Unit 2< Unit 3< Unit 7.

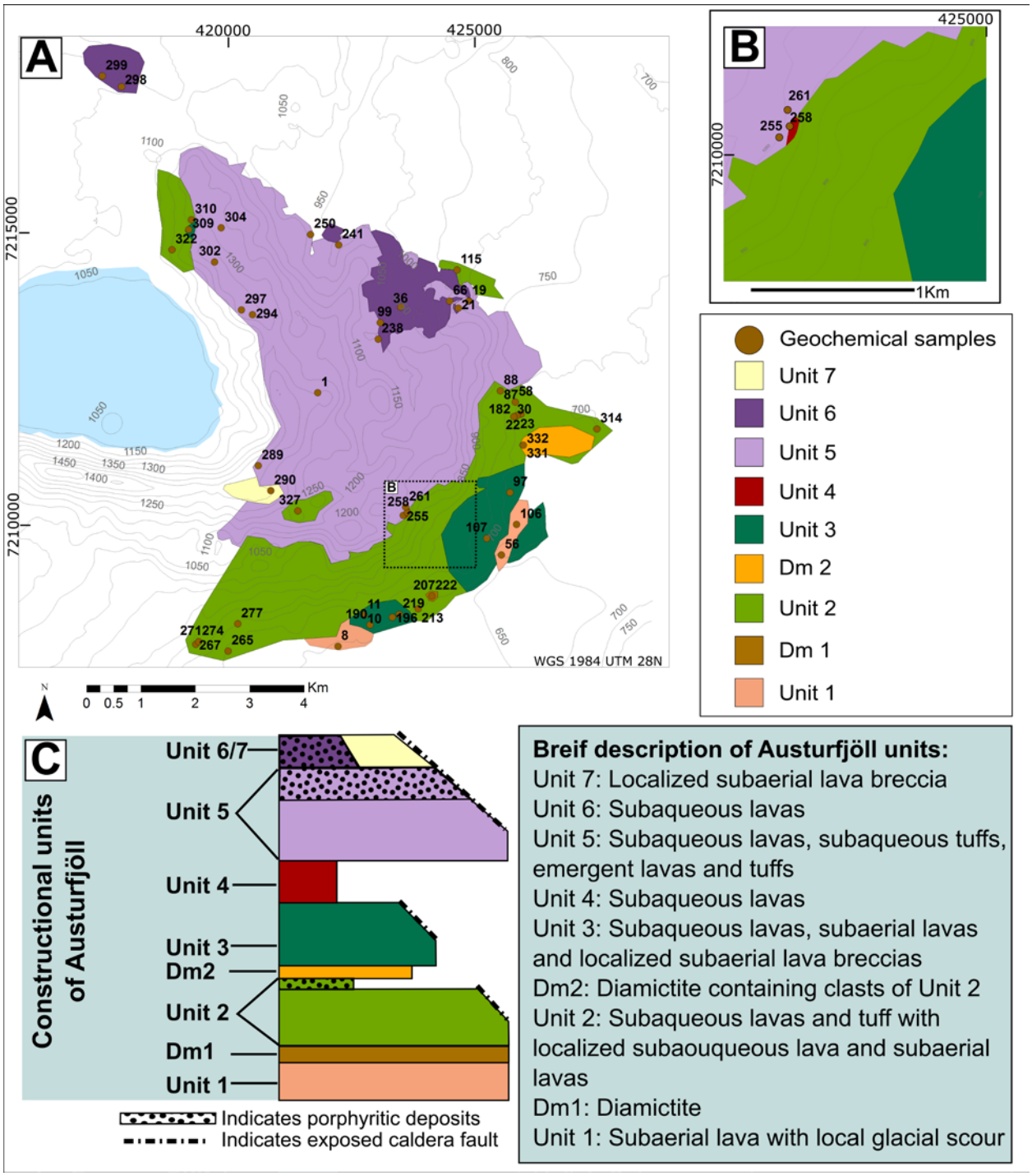

Fig. 10 A) Map of eruptive units at Austurfjöll defined by stratigraphy supplemented with geochemical data. B) Insert region of map to highlight the small exposure of Unit 4. C) Simplified stratigraphic column of the history of the glaciovolcanic massif. Relative width of the column is reflective of unit distribution, while thickness corresponds to unit thickness. The appearance of macro-porphyritic units is noted. The units that are cut by caldera faults are indicated. See Online Resource 2 for cross-sections.

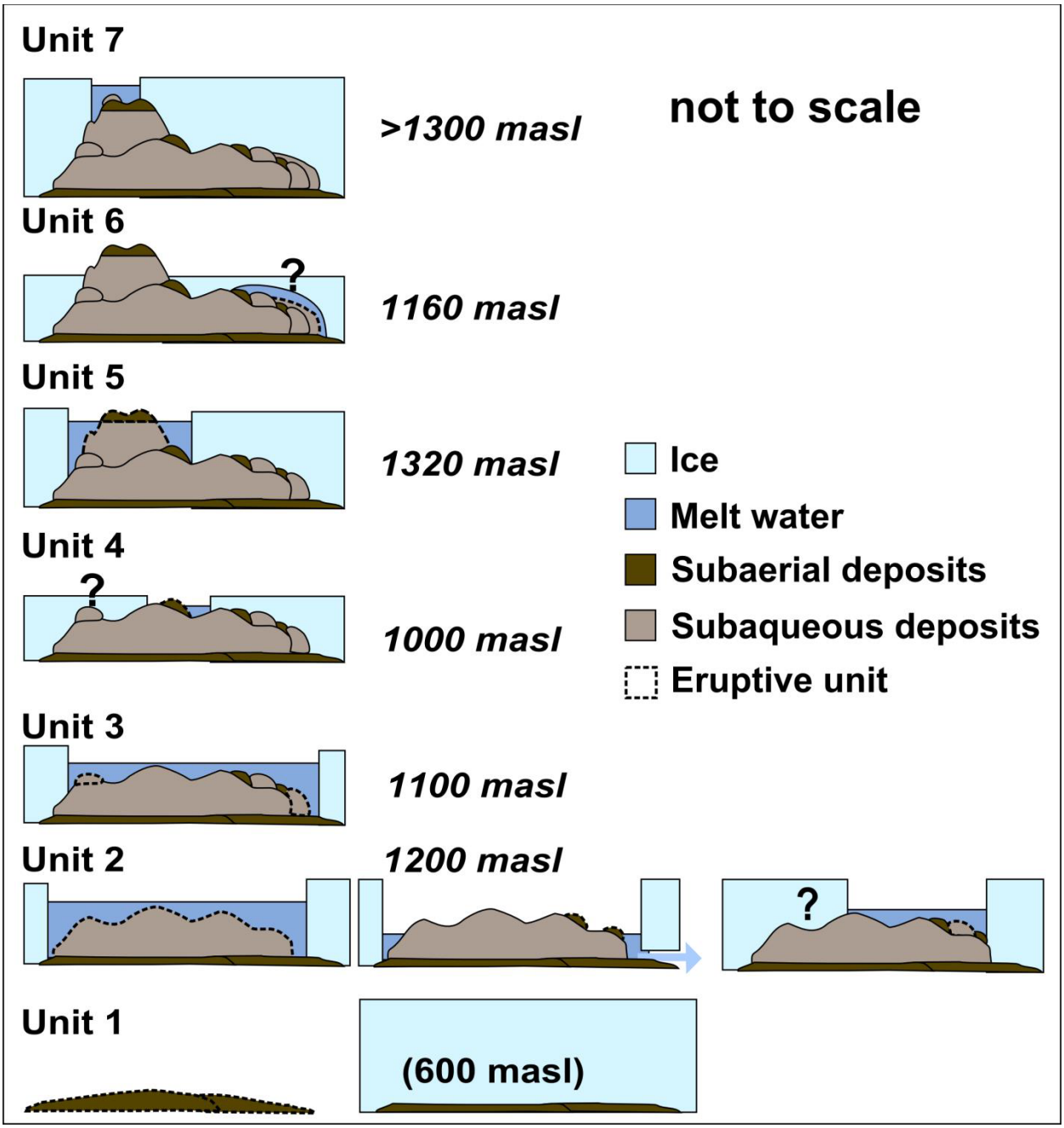

Figure 11: Simplified chronology of relative ice and meltwater positions based on lithofacies mapping and eruptive chronology for Austurfjöll massif using an W-E section. This schematic highlights the variability and recurring nature of meltwater lakes over the massif. The water and ice positions here are minimums, values in italics are maximum elevations of subaqueous deposits for a given unit. Distributions and geometries that involve thicker ice or additional bodies of meltwater are possible. Additional drainage events (as depicted for Unit 2) are also possible. The meltwater is depicted as an open lake due to the large areal extent of the eruptive deposits (Unit 2 & 3). Question marks indicate poorly constrained ice conditions.

Table 1: Lithofacies found at Austurfjöll

Code	General	Description
x= porphyritic		
L	**Lavas**	
Pl_1	Microcrystalline pillows	Regularly stacked pillow forms. Wide range in vesicularity.
Pl_2	Microcrystalline pillows	Irregular pillow forms, may have columnar flow cores. Wide range in vesicularity.
Plx_1	Porphyritic pillows	Regular pillow forms. Displays radial and vertical pipe vesicles. Wide range in pillow core. Crystal population dominated by plagioclase, with minor Cpx.
Plx_2	Porphyritic pillows	Irregular pillow forms, may have columnar flow lobes. Wide range in vesicularity. Phenocryst population dominated by plagioclase, with minor Cpx.
L1	Subaqueous sheet lava	Microcrystalline lava, vesicularity is low, can display columnar joints, and chill margins.
Lx	Porphyritic subaqueous sheet lava	Porphyritic lava flow, vesicularity is low. Can display columnar jointing, and chill margins. Phenocryst population dominated by plagioclase, with minor Cpx.
L2	Subaerial lava	Dense, microcrystalline lava with oxidation and local scoriaceous tops.
Lx2	Porphyritic subaerial lava	Dense, microcrystalline lava with oxidation and local scoriaceous tops. Contains visible phenocrysts of plagioclase feldspar. Phenocryst population dominated by plagioclase, with minor Cpx.
B	**Breccias**	
B1	Microcrystalline pillow breccia	Contains intact pillows and fragments of pillows. Typically angular to subangular. May contain fluidal bombs. Clast to variable clast to matrix support, coarse ash matrix.
Bx1	Porphyritic pillow breccia	Porphyritic pillows and pillow fragments. Phenocryst population dominated by plagioclase, with minor Cpx. Clast to variable clast to matrix support, coarse ash matrix.
B2	Microcrystalline angular block breccia	Contains angular blocks. Clast to variable clast to matrix support, coarse ash matrix.
Bx2	Porphyritic angular block breccia	Porphyritic angular blocks. Phenocryst population dominated by plagioclase, with minor Cpx. Clast to variable clast to matrix support, coarse ash matrix.
B3	Subaerial lava fragment breccia	Fragments of dense subaerial lava. Matrix or clast supported breccia containing coarse ash and lapilli. May include red scoria or porphyritic lithics.
Dia	**Diamictite**	
Dia1	Matrix supported conglomerate, contains glacial clasts	Subrounded to rounded clasts supported in a fine ash matrix. Distinctive striated cobbles and outsized clasts (glacial erratics). Typically on the order of 1 m thick, but not laterally continuous.
Dia2	Matrix supported	Subrounded to rounded clasts supported in a fine ash

	conglomerate	matrix. Glacial characteristics like striated clasts may be present. Thin units that are well bedded, dominated by ash sized particles. Typical deposit thickness is on the order of 50 cm and occurs on glacially scoured surfaces.
Lt	**Lapilli tuffs**	
Lt1	Angular glassy lapilli tuff with pillows and fluidal bombs	Dominated by 2-4 cm diameter angular glass fragments, clast or matrix supported with coarse ash matrix. Outsized clasts include pillow fragments and pillow. Massive, normal grading common.
Lt2	Subrounded lapilli tuff with subangular blocks / bombs no visible phenocrysts	Dominated by subrounded lapilli, clast or matrix supported with outsized clasts of subangular to rounded blocks with a coarse ash matrix. Bedding is inconsistent and weak.
Lt2x	Porphyritic subrounded lapilli tuff with subangular blocks / bombs	Dominated by subrounded lapilli of porphyritic lava and occasional independent crystals up to 1 cm in diameter May be clast- or matrix-supported. Outsized clasts include subangular to rounded blocks. Phenocryst population dominated by plagioclase with minor Cpx.
Lt3	Subaerial component lapilli tuff	Dominated by subrounded lapilli, clast or matrix supported with outsized clasts of bombs and bomb fragments. Coarse ash matrix. Contains armored lapilli, in addition to other subaerial pyroclasts.
Lt3x	Subaerial porphyritic lapilli tuff	Dominated by subrounded lapilli of porphyritic lapilli sized clasts of lava and independent crystals up to 1 cm in diameter May be clast or matrix supported. Outsized clasts include lava blocks and bombs. Coarse ash matrix. Contains armored lapilli, in addition to other subaerial pyroclasts.
Lt4	Heterolithic lapilli tuff	Dominated by 2-4 cm diameter angular lapilli of porphyritic and microcrystalline vesicular clasts. May include red scoria and / or clasts of ash tuff or subaerial lava. Coarse ash matrix supported with outsized clasts of 2-15 cm.
At	**Ash Tuffs**	
At1	Massive coarse ash	Massive coarse ash, with variable palagonitization.
At2	Bedded coarse and fine ash, Laminated ash units	Bedded to laminated unit of coarse ash, fine ash, and occasional silt. Laminations occur in beds 2 cm thick.
At3	Alternating beds of variable grain sizes dominated by ash	Beds of ash, lapilli and block bearing tuffs. Individual beds range between 2 and 15 cm. Weak sedimentary structures on cm scale, such as ripples and scours may occur.
At4	Deformed domains of vitric ash and lapilli	Discrete packets of bedded ash dominated tuffs that have steep dips and convoluted folding that does not match the surrounding bedding. Outsized clasts may range from lapilli to block size.

Table 2: Analysis of stratigraphically constrained Unit 2 as a representative of one geochemically distinct magma batch from Austurfjöll (Unit 2).

Unit	**2**	**2**	**2**	**2**	**2**	**2**	**2**	**2**	**2**	**2**	**2**	**2**	**2**	**2**	**2**	**2**	**2**	**2**	**2**	**2**	**2**	**2**	**2**	**2**	**Unit**	Unit	Analy-
Sample	AG 274	AG 331	AG 58	AG 182	AG 22	AG 314	AG 176	AG 207	AG 327	AG 213	AG 30	AG 58a	AG 58b	AG 87	AG 88	AG 115	AG 23	AG 267	AG 322	AG 277	AG 265	AG 310	AG 271	**mean**	range	tical error
Wt %																											
SiO_2	50.63	50.77	51.13	50.70	50.51	50.64	50.43	51.04	50.43	46.83	50.57	50.13	50.04	51.39	50.23	50.50	50.33	50.46	48.06	52.32	50.33	51.01	50.95	**50.41**	46.83-52.32	1.00
TiO_2	2.52	2.50	2.52	2.51	2.49	2.47	2.51	2.28	2.29	2.33	2.48	2.46	2.45	2.50	2.49	2.47	2.51	2.23	2.31	1.86	2.34	2.22	2.36	**2.40**	1.86-2.52	1.00
Al_2O_3	13.27	13.22	13.33	13.24	13.22	13.19	13.23	13.76	13.84	13.99	13.31	13.19	13.18	13.37	13.28	13.19	13.25	13.68	14.36	13.94	13.62	14.25	13.69	**13.50**	13.18-14.29	1.00
FeO*	14.13	13.87	14.17	14.04	13.79	14.26	14.09	13.50	13.59	13.66	15.79	16.25	16.07	14.83	15.88	15.89	16.06	14.13	13.80	12.14	13.90	12.44	14.20	**14.37**	12.14-16.25	1.00
MnO	0.25	0.23	0.24	0.24	0.24	0.24	0.24	0.23	0.24	0.29	0.25	0.25	0.24	0.25	0.25	0.24	0.25	0.24	0.22	0.20	0.24	0.26	0.25	**0.24**	0.20-0.29	1.00
MgO	5.22	5.29	5.43	5.37	5.42	5.47	5.00	5.72	5.53	5.21	5.22	5.38	5.39	5.40	5.43	5.46	5.20	5.58	5.18	5.56	5.36	5.45	4.94	**5.36**	4.94-5.72	1.00
CaO	10.00	9.92	9.83	9.84	9.95	9.99	9.89	10.40	10.28	10.44	9.95	9.75	9.76	10.03	9.85	9.86	9.92	10.24	10.31	9.87	10.02	10.44	9.46	**10.00**	9.46-10.44	1.00
Na2O	2.52	2.61	2.55	2.59	2.56	2.62	2.58	2.57	2.75	2.56	2.60	2.47	2.52	2.61	2.47	2.54	2.57	2.63	2.41	2.54	2.70	2.51	2.82	**2.58**	2.41-2.82	1.00
K2O	0.48	0.50	0.51	0.49	0.48	0.48	0.48	0.43	0.48	0.19	0.52	0.51	0.53	0.51	0.49	0.54	0.50	0.44	0.37	0.60	0.52	0.38	0.54	**0.48**	0.19-0.60	1.00
P_2O_5	0.28	0.27	0.28	0.27	0.27	0.26	0.28	0.24	0.26	0.27	0.28	0.28	0.28	0.28	0.28	0.27	0.28	0.25	0.27	0.21	0.27	0.26	0.29	**0.27**	0.21-0.29	1.00
Total	99.3	99.2	99.9	99.3	98.9	99.6	98.7	100.2	99.7	95.8	101.1	100.8	100.6	101.3	100.8	101.1	100.9	99.9	97.3	99.2	99.3	99.2	99.5	**99.6**		
ppm																										
Nb	19	19	19	19	19	19	19	17	17	18	20	20	20	20	20	19	20	17	18	15	19	19	19	**19**	17-20	1.00
Rb	9	11	11	10	11	12	10	9	10	2	11	11	11	11	10	10	10	8	6	14	12	10	12	**10**	2-14	1.00
Sr	189	187	186	186	187	183	188	193	214	195	182	178	179	188	181	181	183	201	203	186	214	212	203	**191**	178-214	1.00
Y	41	41	42	41	41	41	41	38	33	34	38	38	38	38	38	37	39	35	34	37	35	37	39	**38**	34-42	1.00
Zr	172	170	174	172	169	165	172	152	150	153	170	170	169	170	169	169	170	150	153	158	157	157	177	**165**	150-172	1.00
Ce	38	39	42	37	39	38	40	32	34	39	56	32	31	36	34	32	57	37	32	34	37	40	36	**38**	31-57	1.00
Cu	130	114	119	111	121	127	123	126	131	128	196	214	202	195	208	169	198	127	129	134	140	130	94	**146**	94-214	0.99
Ni	36	32	32	31	34	35	32	39	34	31	32	49	45	39	35	33	32	33	33	38	31	30	26	**34**	26-49	1.00
Sc	43	43	42	42	41	43	42	43	43	43	42	43	44	45	42	43	41	45	43	38	43	43	41	**43**	38-45	1.00
V	424	421	420	417	422	412	424	401	374	390	418	411	409	423	422	418	416	374	378	332	391	367	345	**400**	332-424	1.00
Zn	127	128	129	130	125	125	127	118	116	118	98	98	102	115	100	96	100	119	114	105	116	118	125	**115**	96-130	1.00

* Total iron measured and reported as FeO. See Online Resource 1.

Analytical error presented is the highest value between the two labs used for this study. See text for detail.

Table 3: Mean composition of eruptive units were first defined by stratigraphic relationships and refined based on chemistry. Incompatible trace elements Nb, Rb, Y, Zr, and Ce were used to establish geochemical fingerprints for eruptive units. In order of increasing enrichment of these incompatible elements: Unit 6, Unit 5, Unit 4, Unit 1, Unit 2, Unit 3 and Unit 7. Trace element ratios highlight the unique combination of concentrations for the units.

	Unit 1		Unit 2		Unit 3		Unit4		Unit 5		Unit 6		Unit 7	
	mean	sd	mean	sd	mean	sd	mean	sd	mean	sd	mean	sd	mean	sd
n	4		23		9		1		11		4		1	
wt%														
SiO_2	50.81	0.22	50.41	1.07	50.31	0.25	49.60	-	50.02	0.70	48.96	0.46	51.72	-
TiO_2	2.15	0.10	2.40	0.15	2.85	0.06	2.15	-	1.86	0.20	1.34	0.09	2.45	-
Al_2O_3	13.71	0.03	13.50	0.37	13.00	0.17	13.60	-	14.74	1.32	19.08	1.03	14.13	-
FeO*	14.30	0.85	14.37	1.13	15.61	0.81	13.94	-	11.90	0.80	8.92	0.79	13.26	-
MnO	0.23	0.00	0.24	0.02	0.25	0.00	0.24	-	0.21	0.01	0.17	0.02	0.23	-
MgO	5.73	0.03	5.36	0.18	4.98	0.12	5.92	-	6.05	0.82	4.78	0.86	3.70	-
CaO	10.37	0.02	10.00	0.25	9.42	0.13	10.79	-	11.78	0.46	13.52	0.22	8.67	-
Na_2O	2.60	0.00	2.58	0.09	2.68	0.04	2.47	-	2.35	0.07	2.00	0.07	2.99	-
K_2O	0.44	0.02	0.48	0.08	0.51	0.06	0.35	-	0.31	0.04	0.19	0.03	0.70	-
P_2O_5	0.23	0.01	0.27	0.02	0.33	0.00	0.23	-	0.20	0.02	0.13	0.01	0.34	-
Total	100.7		99.6		100.0		99.3		99.4		99.1		98.2	
ppm														
Nb	**16**	0.5	**19**	1.3	**22**	0.5	**16**	-	**13**	1.3	**9**	1.1	**23**	-
Rb	**9**	0.3	**10**	2.3	**11**	0.9	**7**	-	**6**	1.0	**4**	0.8	**14**	-
Sr	192	3.4	191	11.1	192	6.8	195	-	205	7.3	221	9.6	215	-
Y	**35**	1.8	**38**	2.6	**44**	2.2	**34**	-	**29**	2.1	**21**	1.6	**47**	-
Zr	**145**	5.9	**165**	8.6	**193**	3.4	**139**	-	**117**	12.0	**79**	9.3	**202**	-
Ce	**38**	13.5	**38**	6.6	**43**	3.4	**31**	-	**26**	1.5	**19**	3.2	**49**	-
Cu	180	48.4	146	36.4	138	28.4	137	-	157	22.3	119	26.4	107	-
Ni	35	4.3	34	5.0	29	1.9	32	-	46	5.2	41	10.8	20	-
Sc	43	0.8	43	1.5	42	1.9	45	-	45	3.3	37	3.0	41	-
V	392	9.5	400	26.8	456	13.1	387	-	335	26.1	251	24.8	335	-
Zn	99	18.3	115	11.4	127	15.1	115	-	96	10.1	70	7.4	167	-
Rb/Nb	0.57		0.54		0.50		0.44		0.47		0.41		0.61	
Zr/Nb	9.18		8.79		8.61		8.69		8.72		8.51		8.78	
Y/Nb	2.22		2.03		1.96		2.13		2.18		2.30		2.04	

*Total iron measured and reported as FeO.

Table 4: Key features and significance of eruptive units described at Austurfjöll, Askja, Iceland

Eruptive unit	Facies	Unique properties	Implications
7	B3	Isolated with no obvious source, subaqueous and subaerial components	Vent was located in area of modern calderas
6	Plx1, Plx2, Ltx2, Atx2	Exclusively porphyritic and subaqueous	Subaqueous activity continued after emergence
5	Pl1, Pl2, Plx1, Plx2, L1, L2, Lx1, B1-3, B1x, Lt1-4, At1-4, G1	Contains diverse componentry, including xenoliths, red scoria, and coated lapilli. G1, B3, Lt4	Records both subaqueous and emergent activity
4	Pl2	Mega pillows, isolated	Limited exposure: burial, or limited eruption
3	Pl1, Pl2, L1, L2, B1-2, Lt1-2, At1- 4	Limited distribution	Mantling paleotopography
2	Pl1, Plx1, Pl2, L2, B1, Lt1-2, At1-3, Dia1	Voluminous pillow sheets	First subaqueous Austurfjöll unit
1	L2, Dia1 , Dia2	Subaerial lava only Glacial scour	Pre-glacial advance

Online resource 1: Complete geochemical dataset (excel spreadsheet).

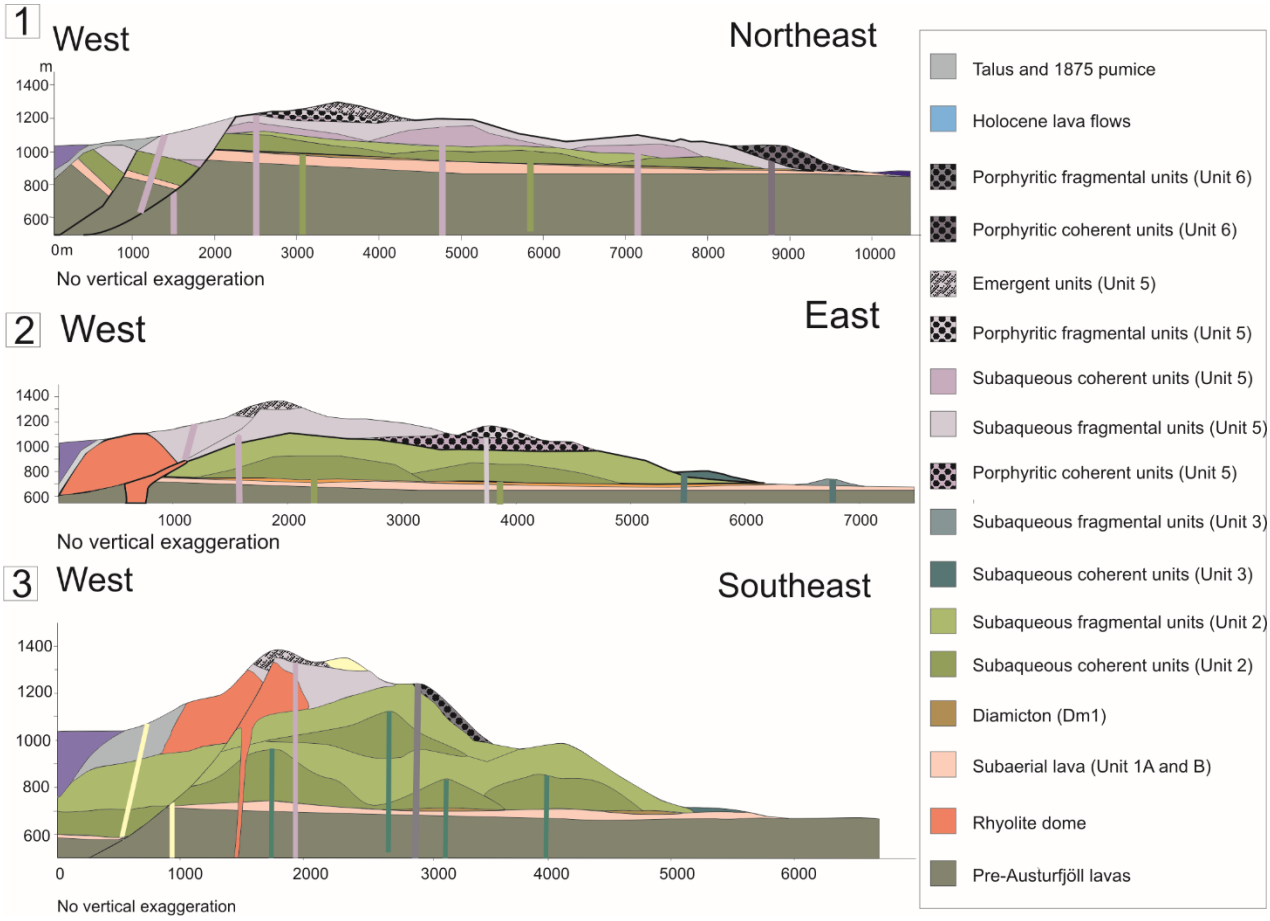

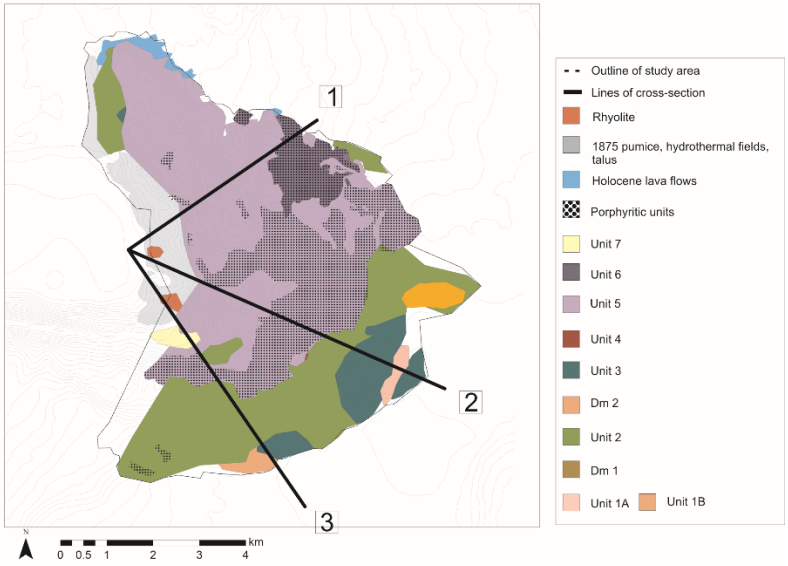

Online resource 2: Example cross-sections through the Austurfjöll massif indicating the development of massif as a sequence of fissure fed pillow lava sheets followed by more explosive fissure ridges. The position of the rhyolite dome is poorly constrained. The position noted here is controlled by exposures and the lack of deformation in over lying unit. The exposures of rhyolite in section 2 and 3 may represent one large deposit or two isolated deposits.